Non-local modelling of freezing and thawing of unsaturated soils

DOI:
10.1016/j.advwatres.2024.104614

Document Version
Final published version

Advances in Water Resources 184 (2024) 104614

Contents lists available at ScienceDirect

Advances in Water Resources

journal homepage: www.elsevier.com/locate/advwatres

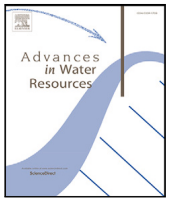

Non-local modelling of freezing and thawing of unsaturated soils

Petr Nikolaev, Andrey P. Jivkov, Lee Margetts, Majid Sedighi *

Department of Solids and Structures, School of Engineering, The University of Manchester, Manchester, UK

ARTICLE INFO

Keywords:
Peridynamics
Heat conduction
Phase change
Stephan problem
Water flow in porous medium
Unsaturated soils

ABSTRACT

A large part of the earth's surface is covered by seasonally or permanently frozen soils. Considering the negative impact of climate change, future development of such regions can be underpinned by mathematical methods for accurate analysis of heat and moisture transport in freezing and thawing soils. Reported in this paper is a novel non-local formulation of water and heat transport in unsaturated soils. The formulation uses bond-based peridynamics (PD) and consists of a set of integral–difference formulations of energy and mass conservation. Specific features of freezing/thawing soils are incorporated by a combination of van Genuthcen and Clausius–Clapeyron relations. Computational results are compared with four sets of laboratory experiments to demonstrate the efficiency of the developed approach. The model can be used to analyse the effect of water flow on heat transfer in soils during thawing of permafrost soils. Further, it can be applied in modelling climate change effects, and can be used for construction of coupled physically justified models of frost heave.

1. Introduction

Freezing and thawing of soils are multi-coupled phenomena involving heat transfer, moisture flow in partially saturated porous media with phase change, and mechanical effects (deformation, cracking). The description of these phenomena involves strong physical and geometrical non-linearities. Decreasing the soil temperature below the water freezing point results in solidification and subsequent volume change. Temperature and pressure gradients drive water migration toward the freezing front, leading to its accumulation in large volumes. Subsequently, the water within the soil pores undergoes freezing, expanding in volume. This expansion exerts pressure on neighbouring soil grains, resulting in their displacement with associated soil volume expansion, i.e. frost heave. If the soil's expansion is constrained, it can induce high pressures, posing risk of damage to buildings, infrastructure, and alterations to the soil's internal structure. The ice crystals formed during freezing merge, creating ice lenses oriented parallel to the freezing front (Kurylyk et al., 2016; Bai et al., 2020). Soil freezing and thawing is characterized by abrupt changes of the physical and mechanical properties between the water phases and the soil with different water phases, by geometric discontinuities, such as inter-phase state boundaries and cracks, and by large non-uniform deformations. These make the mathematical description of the phenomena a challenging task (Amiri et al., 2018).

Existing models for coupled thermal–hydraulic or thermo-hydro-mechanical freezing and thawing are based on the local mathematical formulation of the conservation laws of mass, energy and momenta. For example, freezing and thawing of saturated soils were modelled in Michalowski (1993), Zhang et al. (2018), Tounsi et al. (2020) and Zheng et al. (2022) and of unsaturated soils in Jame and Norum (1980), He et al. (2020b), Chen et al. (2022) and Liu et al. (2023b). These models are phenomenological, i.e., the energy and water mass conservation laws are supplemented with a set of constitutive relationships. For example, the model for freezing and thawing of unsaturated soils (Hansson et al., 2004) supplements the energy and water mass conservation equations with the van Genuchten relationship (van Genuchten, 1980) to define water retention and with the Clausius–Clapeyron equation to define cryo-suction in the frozen region. These constitutive relations were reconsidered in Dall'Amico et al. (2011) and an effective numerical scheme for the model solution was proposed. It was further suggested in Painter (2011) and Painter and Karra (2014) to consider the liquid water content in the frozen zone as governed by the modified form of the soil freezing characteristic curve (SFC). Aspects of vapour redistribution during freezing of relatively dry soils were introduced in Zhang et al. (2016b,a), see also Zhang et al. (2016c). An analysis of the existing mathematical descriptions of freezing soil behaviour was performed in Stuurop et al. (2021), showing that calculations with these models are in general agreement with experiments.

The rapid changes of material properties at the phase change region during soil freezing and thawing as well as the potential growth of cracks pose challenges for numerical schemes based on local formulations of the conservation laws (Hansson et al., 2004; Dall'Amico et al., 2011). The growth of computational power gives the opportunity

* Corresponding author.
E-mail address: majid.sedighi@manchester.ac.uk (M. Sedighi).

https://doi.org/10.1016/j.advwatres.2024.104614
Received 20 April 2023; Received in revised form 27 November 2023; Accepted 1 January 2024
Available online 5 January 2024

to address these challenges by methods based on non-local formulations, which are typically more computationally demanding. One non-local approach with increasing popularity is Peridynamics (PD). In PD, the partial differential equations of any classical local theory are replaced by a set of integral–differential equations (Madenci and Oterkus, 2014), resulting in a mathematically consistent formulation, even in the presence of strong nonlinearities and discontinuities.

The theory of Peridynamics was originally proposed in Silling (2000) and Silling et al. (2007) to describe the mechanical deformations of solids, offering a natural and effective representation of crack development within solid bodies. Subsequently, studies (Bobaru and Duangpanya, 2010, 2012) demonstrated how diffusion problems can be described under the framework of this non-local theory, which later was generalized for the domains with axial and spherical symmetries in Nikolaev et al. (2023). Since then, extensive development of the method has made it possible to propose solutions for various coupled applied problems involving transient heat and/or mass transfer in deformable media. For instance, thermomechanical models of different solids have been considered in Wang et al. (2018, 2019), Chen et al. (2021) and Wang et al. (2022). The interaction between ice and concrete structures that includes freeze-thaw damage was studied in Song et al. (2020, 2021) and Wu et al. (2022). Peridynamics has been applied to geotechnical problems, such as the description of clay erosion by groundwater flow with the appearance of desiccation cracks (Sedighi et al., 2020; Yan et al., 2020, 2021b,a; Liu et al., 2023a), for more details, see the review (Zhou and Wang, 2021). Peridynamics was used to model the corrosion of metals and concrete (Jafarzadeh et al., 2019; Li and Guo, 2021; Jafarzadeh et al., 2022). Models for advection–diffusion and advection–reaction–diffusion problems were proposed in Zhao et al. (2018) and Tian et al. (2023).

The PD description of freezing and thawing was first introduced for analysis of saturated soils (Nikolaev et al., 2022). A model for analysis of frost heave in saturated soils was also proposed (Zhou et al., 2022). These models are not appropriate for analysis of unsaturated soils as they do not consider the water retention characteristics. In addition, the model for frost heave (Zhou et al., 2022) did not consider the effects of heat convection on the energy transfer and did not distinguish isothermal and thermal mass liquid diffusivity in water mass transfer.

In this paper, a peridynamic formulation of heat and water transfer in partially saturated porous media is presented. It uses a modified form of the combined water retention model which includes van Genuchten and Clausius–Clapeyron relationships. A numerical implementation of the new formulation is used to analyse models representing four sets of laboratory experiments. The comparison between calculated and experimental results demonstrates the accuracy of the model. The proposed formulation can be used to describe soil behaviour in the presence of evolving nonlinearities and discontinuities and forms a basis for developing fully coupled thermo-hydro-mechanical models of frost heave.

The paper is structured as follows. In Section 2, the integral formulation of the conservation laws of energy and water mass, supplemented with physically-based constitutive relations, are discussed in detail. These are used in Section 3 to derive the corresponding non-local peridynamic formulations. The peridynamic approach is first verified in Section 4 using two examples solved analytically and by the finite element method. It is then validated in Section 5 using four sets of experiments from published works. Section 6 presents the main conclusions of the paper. Appendix A presents mathematical description of frozen soils' hydraulic and thermal properties that is used in the model. The supplementary equations for the model's numerical implementation are presented in Appendix B.

2. Conservation laws governing the thermo-hydraulic behaviour

A three phase soil system consisting of water, air and solid particles is considered. The water can be in three states: solid (ice), liquid, and gaseous (vapour) as shown in Fig. 1. Generally, water in liquid and gaseous states can be transported.

The impact of vapour transfer can vary significantly depending on the soil type, water content, and temperature regime. According to a parametric study (Zhang et al., 2016c), in certain soils, up to about 90% of water transfer can occur due to vapour flow. However, in such conditions, the total water flux is generally very low. Due to that, even during extended freezing period, the vapour flow is responsible for less than 10%–15% of ice accumulation. Similar findings were provided by multiple papers (He et al., 2018; Zheng et al., 2023). Some numerical studies discovered that, for specific soils, vapour flow has minimal impact on the change in total water content, and it can be fully neglected. For instance, the authors of He et al. (2020b) reached this conclusion for sand and clay, and the authors of Huang and Rudolph (2023) for silt and clay. At the same time, according to Zhang et al. (2016a) and Hou et al. (2023), vapour transfer cannot be ignored if soils are covered by an impermeable layer, leading to the potential developing of the 'canopy' effect. As this study does not aim to describe this particular phenomenon, we will neglect the presence of vapour flow and derive our model following (Hansson et al., 2004; Dall'Amico et al., 2011; Stuurop et al., 2021) by considering that only the movement of liquid water flow contributes to redistribution of moisture in soils and convective heat transfer.

Let $\mathcal{B}$ denote a region of a soil system (solid particles, water and air), and let $\partial\mathcal{B}$ denote its boundary. Both $\mathcal{B}$ and $\partial\mathcal{B}$ can be evolving with time, e.g., due to deformation and/or emergence of cracks. A reference orthogonal coordinate system with axes x, y and z is used to label the points of $\mathcal{B}$, to represent vector quantities, and to orient $\partial\mathcal{B}$ by the outer normal $\mathbf{n}$ to $\mathcal{B}$.

The conservation of a scalar physical property (mass or energy) in the region $\mathcal{B}$ is the equality between the rate of accumulation of the property in $\mathcal{B}$ and the rate of generation of the property in $\mathcal{B}$. The rate of accumulation is given by the Reynolds transport theorem

$$\frac{d}{dt}\int_{\mathcal{B}(t)} p\, dV = \int_{\mathcal{B}} \left(\frac{\partial p}{\partial t} + \nabla\cdot(\mathbf{v}p)\right) dV, \tag{1}$$

where p is the property density, and v is the velocity of a point in $\mathcal{B}$. The rate of generation is given by

$$\int_{\mathcal{B}} r\, dV + \int_{\partial\mathcal{B}} (\mathbf{n}\cdot\mathbf{f})\, dA = \int_{\mathcal{B}} r\, dV + \int_{\mathcal{B}} (\nabla\cdot\mathbf{f})\, dV \tag{2}$$

where r is the rate of production of the property at a point in $\mathcal{B}$, and $\mathbf{f}$ is the flux of the property across $\partial\mathcal{B}$.

The equality of Eqs. (1) and (2) expresses the conservation of the property p, which can be either mass or energy density. If p is mass density (concentration) of a substance, then the term $(\nabla\cdot(\mathbf{v}p))$ in Eq. (1) gives the mass density flux of the substance across the boundary by advection due to matter carrying the substance entering the domain with velocity $\mathbf{v}$, while the term $(\nabla\cdot\mathbf{f})$ in Eq. (2) gives the mass density flux of the substance by diffusion across the boundary due to concentration difference. If p is heat energy density, then the term $(\nabla\cdot(\mathbf{v}p))$ in Eq. (1) gives the flux of heat energy density across the boundary by advection due to substance carrying heat energy density entering the domain with velocity $\mathbf{v}$, while the term $(\nabla\cdot\mathbf{f})$ in Eq. (2) gives the heat energy density flux by diffusion across the boundary due to temperature difference.

The assumptions made for the derivation of the model are:

- the flow of liquid water is defined by Darcy's law and is independently driven by pore water potential and cryosuction, temperature and gravity;
- the influence of vapour flow on the moisture flow in soil is neglected;
- the physical properties of soil components (liquid water, ice, soil grains, and air) are assumed to be homogeneous and isotropic and do not vary with time;

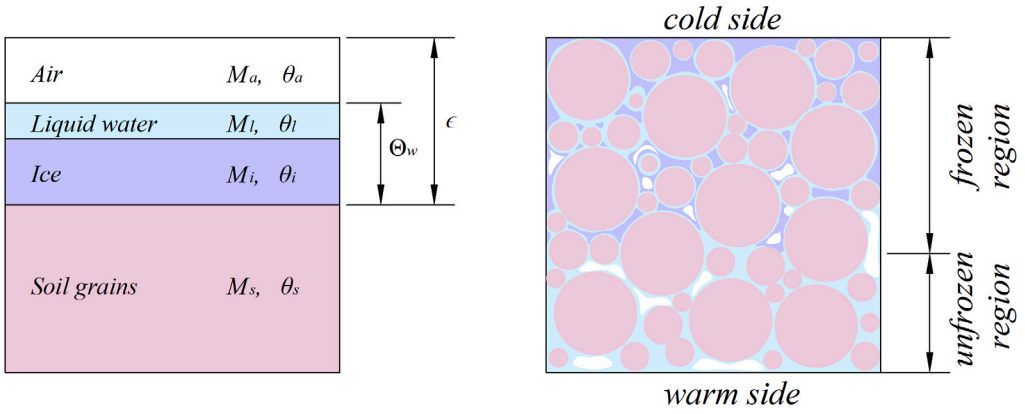

Fig. 1. The structure of freezing soils.

- Porosity is assumed to be constant (i.e., no deformation). As a result, the total water content, which changes due to water migration and phase change, always remains smaller than porosity;
- solidification of water is considered under thermodynamic equilibrium and is defined by a soil freezing characteristic curve that is independent of time and the phase change direction (freezing or thawing);
- the air in pores is considered to be immobile (no contribution to the convective heat transfer).

2.1. Conservation of water mass

The mass of the nth soil system component in a unit volume of $\mathcal{B}$ is denoted by M_n, [kg/m^3]. The mass density of the nth component at a given point of $\mathcal{B}$ is denoted by ρ_n, [kg/m^3]. Assuming that the mass densities of the soil components ρ_n are constant in the unit volume, the volumetric content of the nth component is $\theta_n = M_n/\rho_n$, [m^3/m^3]. To make the description clearer, the subscript n is substituted by the letters i, l, a and s for ice, liquid water, air and soil particles, respectively. With this convention, the porosity of the soil is:

$$\epsilon = \theta_i + \theta_l + \theta_a \quad [\mathrm{m}^3/\mathrm{m}^3], \tag{3}$$

the total mass (gravimetric) water content in unit volume of the region $\mathcal{B}$ is

$$M_w = M_i + M_l \quad [\mathrm{kg}/\mathrm{m}^3], \tag{4}$$

and the total volumetric water content is $\Theta_w = \theta_i + \theta_l$, [m^3/m^3].

The conservation of water mass in the region $\mathcal{B}$ is found from Eqs. (1) and (2) by substituting M_w for p, considering that the possible evolution of $\mathcal{B}$ makes a negligible contribution to the accumulation of water, i.e., $\mathbf{v}M_w \approx 0$, that there is no internal production of water, i.e., $r = 0$, and that flux density is the water flux density $\mathbf{q}_l$, [kg/(m^{2}s)], across $\partial\mathcal{B}$, i.e., $\mathbf{f} = \mathbf{q}_l$. The water conservation is then

$$\int_{\mathcal{B}} \frac{\partial M_w}{\partial t}\, dV = \int_{\mathcal{B}} (\nabla \cdot \mathbf{q}_l)\, dV \tag{5}$$

This conservation law can be formulated in terms of the ice and liquid volumetric contents by dividing both sides by ρ_l:

$$\int_{\mathcal{B}} \left(\frac{\partial \theta_l}{\partial t} + \frac{\rho_i}{\rho_l} \frac{\partial \theta_i}{\partial t} \right) dV = \int_{\mathcal{B}} \frac{1}{\rho_l} \left(\nabla \cdot \mathbf{q}_l \right) dV. \tag{6}$$

For the case of vertical one-dimensional water transfer in soils, which will be used later in the work, Eq. (6) is simplified:

$$\int_{\mathcal{B}} \left(\frac{\partial \theta_l}{\partial t} + \frac{\rho_i}{\rho_l} \frac{\partial \theta_i}{\partial t} \right) dV = \int_{\mathcal{B}} \left(\frac{\partial}{\partial z} \frac{q_l}{\rho_l} \right) dV. \tag{7}$$

Following the approach developed for unfrozen soils (Philip and De Vries, 1957), the 1D water flux density is given by Darcy's law:

$$\frac{q_l}{\rho_l} = K_l \frac{\mathrm{d}\Phi}{\mathrm{d}z} \tag{8}$$

where K_l is the unsaturated hydraulic conductivity, [m/s], and Φ is the total soil water potential, [m], which can be represented as $\Phi = \Psi + z$, where Ψ, [m], is the soil matrix water potential.

Based on laboratory studies of the behaviour of unfrozen unsaturated soils, it has been proposed that $\Psi = f(T, \theta_l)$ (Philip and De Vries, 1957; Nassar and Horton, 1989). Due to the presence of solid ice in frozen soils, this function should be modified to $\Psi = f(T, \Theta_w)$ and should take into account the complex physics of pore water retention and the appearance of cryosuction that is associated with coexistence of liquid and solid water at a negative temperature. Mathematical forms of $f(T, \Theta_w)$ have been proposed, e.g. Taylor and Luthin (1978), Hansson et al. (2004) and Li et al. (2010). This study uses a modified form that corresponds to the semi-empirical approach discussed in Stuurop et al. (2021), see also Dall'Amico et al. (2011), Painter and Karra (2014) and Chen et al. (2022). In this case, Ψ can be assumed to be the sum of two independent functions:

$$\Psi = \Psi_\Theta + \Psi_T, \tag{9}$$

where, $\Psi_\Theta = f(\Theta_w(z), T(z))$ is the soil pore water potential due to the water retention forces, and $\Psi_T = f(T(z))$, is associated with the appearance of cryosuction. Ψ_Θ is defined by considering capillarity forces as a function of surface tension of pore water, σ, [kg/s^2] (Philip and De Vries, 1957). Alternatively other empirical, semi-empirical or analytical theories, e.g. Kurylyk and Watanabe (2013), Vereecken et al. (2016) and Santoyo and Baser (2022), can be adopted in the model. The value of σ can be defined by Eq. (A.4). In the present study, Ψ_Θ is described by the van Genuchten semi-empirical model (van Genuchten, 1980), and has the form of Eq. (A.1). It allows us to compare the modelling results with a broad range of available experimental data sets that include required empirical model parameters. At thermodynamic equilibrium, Ψ_T is defined by the Clausius–Clapeyron Eq. (A.2).

In such case, the total space derivative of Eq. (9) can be represented in a form:

$$\frac{\mathrm{d}\Psi}{\mathrm{d}z} = \frac{\partial \Psi_\Theta}{\partial z} + \left(\frac{\partial \Psi_\Theta}{\partial T} + \frac{\partial \Psi_T}{\partial T} \right) \frac{\partial T}{\partial z} \tag{10}$$

In the developed model, the form of Ψ_Θ in the term $\partial\Psi_\Theta/\partial z$ is defined according to the van Genuchten semi-empirical theory, Eq. (A.1). However, this equation neglects the influence of the temperature on the change of soil water potential, as it does not include T as an equation parameter. Due to that, the value of Ψ_Θ for the term $\partial\Psi_\Theta/\partial T$ can be defined following the classical models (Philip and De Vries, 1957; Hansson et al., 2004) based on the change of capillarity forces.

The relation for Ψ_T of the term $\partial\Psi_T/\partial T$ is chosen in a form of the Clausius–Clapeyron Eq. (A.2). The derivative with temperature is:

$$\frac{\partial\Psi_\Theta}{\partial T}+\frac{\partial\Psi_T}{\partial T}=\begin{cases}\frac{\Psi}{\sigma}\frac{\mathrm{d}\sigma}{\mathrm{d}T}+\frac{L_i}{gT_f}, & \text{if} \quad T<T_f\\ \frac{\Psi_\Theta}{\sigma}\frac{\mathrm{d}\sigma}{\mathrm{d}T}, & \text{if} \quad T\geq T_f\end{cases} \tag{11}$$

where L_i is the latent heat of water solidification, [J/kg]; T_f is the freezing temperature of pore water, [K]; g is the gravity acceleration, [m/s^2].

Substitution of Eqs. (10) and (11) into Eq. (8) gives:

$$q_l=K_l\rho_l\left(\frac{\partial\Psi_\Theta}{\partial z}+1\right)+K_l\rho_l\frac{\partial\Psi_T}{\partial T}\frac{\partial T}{\partial z}=D_{l,\Psi}\left(\frac{\partial\Psi_\Theta}{\partial z}+1\right)+D_{l,T}\frac{\partial T}{\partial z} \tag{12}$$

where $D_{l,T}$ is the modified thermal mass liquid diffusivity for frozen and unfrozen conditions, [kg/(m s K)], and $D_{l,\Psi}=K_l\rho_l$ is the isothermal mass liquid diffusivity (conductivity), [kg/(m^{2}s)].

In the experimental study (Nimmo and Miller, 1986), it has been originally observed that the second term in Eq. (12) cannot accurately predict the water flux caused by the presence of temperature gradient and underestimates the experimental data. In addition to the temperature-induced change in surface tension, there are other temperature-related factors associated with the type of soil, water content, and flow regime that affect the water flux. A special empirical gain factor $G_{\Psi T}$ was proposed to be introduced into the model that accounts for all effects cumulatively. In this case, the thermal liquid diffusivity can be defined as:

$$D_{l,T}=\begin{cases}K_l\rho_l\left(G_{\Psi T}\frac{\Psi}{\sigma}\frac{\mathrm{d}\sigma}{\mathrm{d}T}+\frac{L_i}{gT_f}\right), & \text{if} \quad T<T_f\\ K_l\rho_l G_{\Psi T}\frac{\Psi_\Theta}{\sigma}\frac{\mathrm{d}\sigma}{\mathrm{d}T}, & \text{if} \quad T\geq T_f.\end{cases} \tag{13}$$

Based on the analysis of laboratory experiments it has been proposed that the gain factor is constant and equals 7 for sandy soils (Noborio et al., 1996). In many later studies, e.g. Zhang et al. (2016c) and Zheng et al. (2021), this value has been used also for other types of soils.

The water conservation equation in 1D water transfer becomes:

$$\int_B\left(\frac{\partial\theta_l}{\partial t}+\frac{\rho_i}{\rho_l}\frac{\partial\theta_i}{\partial t}\right)dV=\int_B\frac{1}{\rho_l}\frac{\partial}{\partial z}\left[D_{l,\Psi}\left(\frac{\partial\Psi_\Theta}{\partial z}+1\right)+D_{l,T}\frac{\partial T}{\partial z}\right]dV \tag{14}$$

If the terms under the integrals are locally continuous, the conservation law can be written in a differential form:

$$\frac{\partial\theta_l}{\partial t}+\frac{\rho_i}{\rho_l}\frac{\partial\theta_i}{\partial t}=\frac{1}{\rho_l}\frac{\partial}{\partial z}\left[D_{l,\Psi}\left(\frac{\partial\Psi_\Theta}{\partial z}+1\right)+D_{l,T}\frac{\partial T}{\partial z}\right], \tag{15}$$

which is the local (strong) formulation of water mass transfer. A similar formulation was derived for the case of a two-phase system (liquid water and vapour) in Nassar and Horton (1989) and Nassar and Horton (1992), with the difference that $\partial\theta_l/\partial z$ was used instead of $\partial\Psi/\partial z$. The present formulation is in accord with more recent studies that consider soil freezing (Hansson et al., 2004; Zhang et al., 2016b; Zheng et al., 2021) following Noborio et al. (1996).

2.2. Conservation of heat

The rate of heat accumulation in $\mathcal{B}$ is found from Eq. (1) by substituting p with the heat density H, [J/m^3], considering that heat is accumulated by advection by the flowing water, i.e., $\mathbf{v}=\mathbf{q}_l$, and that there is latent heat of solidification. The heat accumulation is given by

$$\frac{\mathrm{d}}{\mathrm{d}t}\int_{\mathcal{B}(t)}H\,dV=\int_{\mathcal{B}}\left(\frac{\partial H}{\partial t}-\nabla\cdot[L_i+C_l(T-T_0)]\mathbf{q}_l\right)dV \tag{16}$$

where T_0 is the reference temperature, [K], taken to be constant and equal to the freezing temperature of pure water (Dall'Amico et al., 2011); L_i is the latent heat of water solidification, [J/kg], and C_l is the specific heat capacity of liquid water, [J/(kg K)]. In the present study, it is assumed that the thermo-physical parameters of the soil components are constant.

The rate of heat generation in $\mathcal{B}$ is found from Eq. (2) by substituting p with the heat density H, [J/m^3], assuming that the rate of internal heat generation is zero, i.e., $r=0$, and noting that the flux density is the (conductive) heat flux density $\mathbf{q}_h$, [W/m^2], across $\partial\mathcal{B}$, i.e., $\mathbf{f}=\mathbf{q}_h$. The rate of heat generation is then

$$\int_{\partial B}\mathbf{n}\cdot\mathbf{q}_h\,dA=\int_{\mathcal{B}}\left(\nabla\cdot\mathbf{q}_h\right)dV. \tag{17}$$

where the divergence (Gauss's) theorem has been used.

The integral form of the heat conservation equates Eqs. (16) and (17) to give the heat transfer by conduction and advection:

$$\int_{\mathcal{B}}\left(\frac{\partial H}{\partial t}-\nabla\cdot[L_i+C_l(T-T_0)]\mathbf{q}_l\right)dV=\int_{\mathcal{B}}\left(\nabla\cdot\mathbf{q}_h\right)dV \tag{18}$$

For heat transfer only in vertical direction, Eq. (18) is simplified:

$$\int_{\mathcal{B}}\left(\frac{\partial H}{\partial t}-\frac{\partial}{\partial z}\left\{[L_i+C_l(T-T_0)]q_l\right\}\right)dV=\int_{\mathcal{B}}\frac{\partial q_h}{\partial z}dV \tag{19}$$

The total heat content H in a unit volume of soil region $\mathcal{B}$, neglecting the effect of differential heat of wetting, can be defined by Eq. (A.8). Then, following the approach for two-phase systems (water+vapour) presented in Nassar and Horton (1992), where the thermo-physical properties of soil components are assumed to be constant, the rate of heat content change is:

$$\frac{\partial H}{\partial t}=C_{av}\frac{\partial T}{\partial t}+\rho_iC_i(T-T_0)\frac{\partial\theta_i}{\partial t}+\left[L_i+C_l(T-T_0)\right]\rho_l\frac{\partial\theta_l}{\partial t} \tag{20}$$

where $C_{av}(\theta_i,\theta_l,\theta_a)=\rho_sC_s(1-\epsilon)+\rho_iC_i\theta_i+\rho_lC_l\theta_l+\rho_a\theta_aC_a$ is the volumetric heat capacity of unsaturated soils, [J/(m^{3}K)]; C_n denote the specific heat capacities of different phases, [J/(kg K)].

The 1D conductive heat flux is described by the Fourier law:

$$q_h=-\Lambda_{av}\frac{\partial T}{\partial z} \tag{21}$$

where Λ_{av} is the average thermal conductivity of unsaturated soil, [W/(m K)], that can be defined, for example, by Eqs. (A.9) or (A.10).

With the assumptions used for deriving Eq. (20), the spatial derivative of the conductive heat flux density is:

$$\frac{\partial q_h}{\partial z}=-\frac{\partial}{\partial z}\left(\Lambda_{av}\frac{\partial T}{\partial z},\right) \tag{22}$$

and the spatial derivative of the advective heat transfer is:

$$\frac{\partial}{\partial z}\left\{[L_i+C_l(T-T_0)]q_l\right\}=C_lq_l\frac{\partial T}{\partial z}+\left[L_i+C_l(T-T_0)\right]\frac{\partial q_l}{\partial z} \tag{23}$$

Substituting Eqs. (20), (22) and (23) into Eq. (19) and taking into account the definition of $\partial q_l/\partial z=\rho_l\partial\theta_l/\partial t+\rho_i\partial\theta_i/\partial t$ gives the general 1D integral form of heat conservation:

$$\int_{\mathcal{B}}\left(C_{av}\frac{\partial T}{\partial t}+\rho_i\left[(T-T_0)(C_i-C_l)-L_i\right]\frac{\partial\theta_i}{\partial t}-C_lq_l\frac{\partial T}{\partial z}\right)dV=-\int_{\mathcal{B}}\frac{\partial}{\partial z}\left(\Lambda_{av}\frac{\mathrm{d}T}{\mathrm{d}z}\right)dV \tag{24}$$

If the terms under the integrals are locally continuous, the 1D heat conservation can be written in a differential form:

$$C_{av}\frac{\partial T}{\partial t}+\rho_i\left[(T-T_0)(C_i-C_l)-L_i\right]\frac{\partial\theta_i}{\partial t}=-\frac{\partial}{\partial z}\left(\Lambda_{av}\frac{\mathrm{d}T}{\mathrm{d}z}\right)+C_lq_l\frac{\partial T}{\partial z} \tag{25}$$

This form of energy conservation was used previously in Dall'Amico et al. (2011) and Stuurop et al. (2021, 2022). Here, the term $\left[L_i-(T-T_0)(C_i-C_l)\right]$ represents the effective latent heat of solidification, i.e. the reduction of the latent heat due to the depression of the melting point of water, see e.g. Güémez et al. (2001) and Kumano et al. (2007). In other studies, e.g. Hansson et al. (2004), Sheshukov and Nieber (2011) and Zhang et al. (2016c), the term $(T-T_0)(C_i-C_l)$ was not taken into account.

It should be noted that the heat and water mass conservation equations can be derived in a similar manner for systems containing all three

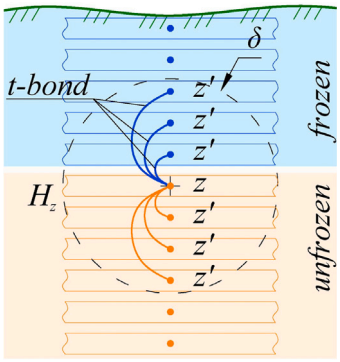

Fig. 2. Illustration of phase regions, particle horizons and transport bonds ('t-bonds').

states of water (ice, liquid water, vapour). However, such a derivation leads to the appearance of several additional terms both for L_i and L_c (the latent heat of vaporization, [J/kg]), which are also usually not taken into account, see e.g. Zhang et al. (2016b,c) and He et al. (2020b). Moreover, the temperature of water condensation T_c, [K], and L_c change significantly and cannot be considered constants. This makes mathematically rigorous construction of the energy conservation equation for such three water state systems challenging.

3. Bond-based peridynamics formulations of conservation laws

A soil body occupying a region $\mathcal{B}$ is considered as a collection of horizontal layers (peridynamic particles) with associated thickness and mass, see Fig. 2. In the bond-based peridynamics, the term 'bond' refers to the interactions between two soil layers, located at depths z and z'. The bond between interacting soil layers will be referred to as a 't-bond' (for transport bond). The peridynamic heat and fluid flux per unit volume along a 't-bond' depends on the distance between the layers z and z'. The soil layer z interacts with (and is connected to) all soil layers z' within a certain finite region $\mathcal{H}_z$, called the horizon of soil layer z. In the present paper, the horizon is symmetric with respect to the layer z. The thickness of the layer and the size of the horizon are denoted by Δ_z, and $\delta = m\Delta_z$, respectively, where m is the relative size of the horizon. Generally, the value of m can be chosen arbitrarily, however, in problems of diffusion, it is usually set to 3 or 4, as shown in Nikolaev et al. (2022, 2023), Yan et al. (2020) and Tian et al. (2023). Such values were justified by parametric studies in Chen and Bobaru (2015) and Jabakhanji and Mohtar (2015), which indicated that smaller m ensure better accuracy.

3.1. PD formulation for water flow

Modifying the approach (Katiyar et al., 2014), the Peridynamics liquid water mass flux between two interacting soil layers z and z' per unit volume is given by:

$$\begin{aligned}\overline{J_l}\left(z',z,t\right) =& D_{l,\Psi}\left(z',z,t\right)\frac{\boldsymbol{\Phi}_\Theta\left(z',t\right)-\boldsymbol{\Phi}_\Theta\left(z,t\right)}{\|z'-z\|}\cdot\frac{z'-z}{\|z'-z\|}+\\ & D_{l,T}\left(z',z,t\right)\frac{T\left(z',t\right)-T\left(z,t\right)}{\|z'-z\|}\cdot\frac{z'-z}{\|z'-z\|}\end{aligned} \tag{26}$$

where $\overline{J_l}\left(z',z,t\right)$ is the volumetric mass flux of water and vapour; $\boldsymbol{\Phi}_\Theta\left(z,t\right)$ and $\boldsymbol{\Phi}_\Theta\left(z',t\right)$ are the soil water potentials at soil layers z and z', respectively, that depends on the total water content and defined under the framework of the van Genuchten (1980) theory; $T\left(z,t\right)$ and $T\left(z',t\right)$ are the temperatures at the soil layers z and z', respectively; $D_{l,\Psi}\left(z',z,t\right)$ and $D_{l,T}\left(z',z,t\right)$ are the average isothermal and thermal diffusivity of liquid water of the 't-bond' between the soil layers z and z', which can be defined by averaging the diffusivity values of the two connected soil layers. It can be done by application of the arithmetic mean (Bobaru and Duangpanya, 2012; Yan et al., 2021a):

$$\begin{aligned}D_{l,\Psi}\left(z',z,t\right) &= \frac{D_{l,\Psi}\left(z,t\right)+D_{l,\Psi}\left(z',t\right)}{2}\\ D_{l,T}\left(z',z,t\right) &= \frac{D_{l,T}\left(z,t\right)+D_{l,T}\left(z',t\right)}{2}\end{aligned} \tag{27}$$

harmonic mean (Nikolaev et al., 2022, 2023):

$$\begin{aligned}D_{l,\Psi}\left(z',z,t\right) &= \frac{2D_{l,\Psi}\left(z,t\right)D_{l,\Psi}\left(z',t\right)}{D_{l,\Psi}\left(z,t\right)+D_{l,\Psi}\left(z',t\right)}\\ D_{l,T}\left(z',z,t\right) &= \frac{2D_{l,T}\left(z,t\right)D_{l,T}\left(z',t\right)}{D_{l,T}\left(z,t\right)+D_{l,T}\left(z',t\right)}\end{aligned} \tag{28}$$

or geometric mean:

$$\begin{aligned}D_{l,\Psi}\left(z',z,t\right) &= \sqrt{D_{l,\Psi}\left(z,t\right)D_{l,\Psi}\left(z',t\right)}\\ D_{l,T}\left(z',z,t\right) &= \sqrt{D_{l,T}\left(z,t\right)D_{l,T}\left(z',t\right)}\end{aligned} \tag{29}$$

The harmonic and geometric means ensure that when the difference between the diffusivities of layers z and z' is substantial, the average diffusivity of the t-bond will be much closer to the lower of the two values. Consequently, the predicted water flux between these two layers will be much smaller than in the case of arithmetic averaging. This property is particularly important when describing cryosuction-driven water transfer in t-bonds crossing the moving phase change boundary, with one side of the t-bond located in the frozen soil and having nearly zero diffusivity. The application of arithmetic averaging for the hydraulic properties of these interfacial t-bonds can lead to the over-accumulation of water in the frozen area. Therefore, for such soils, either harmonic averaging or geometric averaging should be used. It should be noted that if the impedance factor is used to adjust the hydraulic conductivity of the frozen soil, as is done in this paper by Eq. (A.7), its empirical shape parameter η can be chosen in a way that the diffusivities of the interfacial t-bonds defined by both averaging methods are equal, making them interchangeable in many practical problems.

Based on Eq. (7), and following Katiyar et al. (2014) and Yan et al. (2020), the water mass conservation within a single t-bond that connect the soil layers z and z' is written as:

$$\rho_l\frac{\partial}{\partial t}\theta_l\left(z',z,t\right)+\rho_i\frac{\partial}{\partial t}\theta_i\left(z',z,t\right)=\frac{\overline{J_l}\left(z',z,t\right)}{\|z'-z\|} \tag{30}$$

Eq. (30) is integrated over the horizon of z to obtain the mass conservation in layer z due to flow along all t-bonds within its horizon $\mathcal{H}_z$:

$$\rho_l\int_{\mathcal{H}_z}\frac{\partial}{\partial t}\theta_l\left(z',z,t\right)\mathrm{d}V_{z'}+\rho_i\int_{\mathcal{H}_z}\frac{\partial}{\partial t}\theta_i\left(z',z,t\right)\mathrm{d}V_{z'}=\int_{\mathcal{H}_z}\frac{\overline{J_l}\left(z',z,t\right)}{\|z'-z\|}\mathrm{d}V_{z'} \tag{31}$$

Following Yan et al. (2020), the relationship between the volumetric water content in the soil layer z and time t and the average water content in all the t-bonds connected to z is given by:

$$\int_{\mathcal{H}_z}\frac{\partial\theta_l\left(z',z,t\right)}{\partial t}\mathrm{d}V_{z'}=\frac{\partial\theta_l\left(z,t\right)}{\partial t}V_{\mathcal{H}_z} \tag{32}$$

The same relationship holds for the ice content:

$$\int_{\mathcal{H}_z}\frac{\partial\theta_i\left(z',z,t\right)}{\partial t}\mathrm{d}V_{z'}=\frac{\partial\theta_i\left(z,t\right)}{\partial t}V_{\mathcal{H}_z} \tag{33}$$

By introduction of micro-diffusivity parameters $d_{l,\Psi}=D_{l,\Psi}/V_{\mathcal{H}_z}$ and $d_{l,T}=D_{l,T}/V_{\mathcal{H}_z}$, the mass conservation in soil layer z can be rewritten

as:

$$\frac{\partial\theta_l(z,t)}{\partial t}+\frac{\rho_i}{\rho_l}\frac{\partial\theta_i(z,t)}{\partial t}= \int_{\mathcal{H}_z} d_{l,\Psi}\left(z',z,t\right)\frac{\boldsymbol{\Phi}_\Theta\left(z',t\right)-\boldsymbol{\Phi}_\Theta(z,t)}{\|z'-z\|^2}\mathrm{d}V_{z'}+ \int_{\mathcal{H}_z} d_{l,T}\left(z',z,t\right)\frac{T\left(z',t\right)-T(z,t)}{\|z'-z\|^2}\mathrm{d}V_{z'} \tag{34}$$

Following Zhao et al. (2018), the micro-diffusivity parameters $d_{l,\Psi}$ and $d_{l,T}$ can be presented as:

$$d_{l,\Psi}\left(z',z,t\right)=\frac{D_{l,\Psi}\left(z',z,t\right)}{\delta} \qquad d_{l,T}\left(z',z,t\right)=\frac{D_{l,T}\left(z',z,t\right)}{\delta} \tag{35}$$

The liquid velocity through porous unsaturated media is defined using the approach proposed in Katiyar et al. (2014). The velocity at layer z is determined by considering the moisture flow through all t-bonds with layers z' that have higher soil water potential and temperature. These are layers within a restricted horizon denoted by $\boldsymbol{\mathcal{H}}_{\mathbf{z}}^{+,\boldsymbol{\Phi}}$ and $\boldsymbol{\mathcal{H}}_{\mathbf{z}}^{+,\mathbf{T}}$ respectively. Thus:

$$U_l(z,t)=-\int_{\boldsymbol{\mathcal{H}}_{\mathbf{z}}^{+,\boldsymbol{\Phi}}} d_{l,\Psi}\left(z',z,t\right)\frac{\boldsymbol{\Phi}_\Theta\left(z',t\right)-\boldsymbol{\Phi}_\Theta(z,t)}{\|z'-z\|}\cdot\frac{z'-z}{\|z'-z\|}\mathrm{d}V_{z'}- \int_{\boldsymbol{\mathcal{H}}_{\mathbf{z}}^{+,\mathbf{T}}} d_{l,T}\left(z',z,t\right)\frac{T\left(z',t\right)-T(z,t)}{\|z'-z\|}\cdot\frac{z'-z}{\|z'-z\|}\mathrm{d}V_{z'} \tag{36}$$

3.2. PD formulation for heat transfer with change of water state

According to Nikolaev et al. (2023), the heat flux along the t-bond $\overline{J_h}\left(z',z,t\right)$ from one soil layer to another can be defined as:

$$\overline{J_h}\left(z',z,t\right)=-\Lambda_s\left(z',z,t\right)\frac{T\left(z',t\right)-T(z,t)}{\|z'-z\|}\cdot\frac{z'-z}{\|z'-z\|}+ C_l\rho_l U_l\left(z',z,t\right)\left[T\left(z',t\right)-T(z,t)\right]\cdot\frac{z'-z}{\|z'-z\|} \tag{37}$$

where $T\left(z',t\right)$ and $T(z,t)$ are the temperature at soil layers z and z' respectively; $\frac{z'-z}{\|z'-z\|}$ is the unit vector along the 't-bond'; $\Lambda(z,z',t)$ is the average thermal conductivity of the material at soil layers z and z' respectively; and $U_l\left(z',z,t\right)=(U_l\left(z',t\right)+U_l(z,t))/2$ is the average velocity along the t-bond. The average thermal conductivity can be defined in a way similar to what was discussed regarding hydraulic diffusivity as arithmetic, harmonic, and geometric means of the heat conductivities of layers z and z':

$$\Lambda(z,z',t)=\frac{\Lambda(z,t)+\Lambda(z',t)}{2} \tag{38}$$

$$\Lambda(z,z',t)=\frac{2\Lambda(z,t)\Lambda(z',t)}{\Lambda(z,t)+\Lambda(z',t)} \tag{39}$$

$$\Lambda(z,z',t)=\sqrt{\Lambda(z,t)\Lambda(z',t)} \tag{40}$$

The difference between the heat conductivities of frozen and unfrozen soils is relatively small. Because of that, the choice of the averaging technique does not significantly impact the calculation results.

Following Bobaru and Duangpanya (2010, 2012) and extending their approach by taking into account Eq. (24), the energy conservation in a 't-bond' between two soil layers z and z' can be defined by

$$\overline{(\rho C)_{av}}(z',z,t)\frac{\partial}{\partial t}\overline{T}(z',z,t)+ \rho_i\left[(C_i-C_l)(\overline{T}(z',z,t)-T_0)-L_i\right]\frac{\partial\theta_i(z',z,t)}{\partial t}=\frac{\overline{J_h}\left(z',z,t\right)}{\|z'-z\|} \tag{41}$$

where $\overline{T}(z',z,t)$ is the average temperature of the t-bond between soil layers z and z', and $\overline{(\rho C)_{av}}(z',z,t)$ is the average equivalent heat capacity of the t-bond. Combining Eqs. (37) and (41) gives the energy conservation equation in the 't-bond'.

The conservation of energy at the soil layer z involves the fluxes in all the t-bonds adjacent to z (t-bonds to particles within the horizon $\mathcal{H}_z$) and is obtained by integrating Eq. (41) over the horizon $\mathcal{H}_z$. If the properties in the horizon are assumed to be defined by the properties of the layer z, the temperature evolution at layer z can be calculated. Introducing the micro-conductivity $\lambda_s=\Lambda_s/V_{\mathcal{H}_z}$ and the micro-velocity $u_l=U_l/V_{\mathcal{H}_z}$ (Zhao et al., 2018), Eqs. (32)–(41) can be written as:

$$\overline{(\rho C)_{av}}(z,t)\frac{\partial}{\partial t}\overline{T}(z,t)+\rho_i\left[(C_i-C_l)(\overline{T}(z,t)-T_0)-L_i\right]\frac{\partial\theta_i(z,t)}{\partial t}= -\int_{\mathcal{H}_z}\lambda_s\left(z',z,t\right)\frac{T\left(z',t\right)-T(z,t)}{\|z'-z\|^2}\mathrm{d}V_{z'}+ \int_{\mathcal{H}_z} C_l\rho_l u_l\left(z',z,t\right)\frac{\left[T\left(z',t\right)-T(z,t)\right]}{\|z'-z\|}\mathrm{d}V_{z'} \tag{42}$$

The micro-conductivity λ_s and the micro-velocity u_l can be presented following Zhao et al. (2018) as:

$$\lambda_s\left(z',z,t\right)=\frac{\Lambda_s\left(z',z,t\right)}{\delta} \qquad u_l\left(z',z,t\right)=\frac{U_l\left(z',z,t\right)}{2\delta} \tag{43}$$

3.3. Numerical implementation

The numerical solution of the developed PD model is obtained by discretization of the domain to a uniform grid with its step size equal to the layer thickness.

The spatial discretization of the mass conservation Eq. (34) is:

$$\frac{\partial\theta_l\left(z_i,t\right)}{\partial t}+\frac{\rho_i}{\rho_l}\frac{\partial\theta_i\left(z_i,t\right)}{\partial t}=\sum_p d_{l,\Psi}\left(z_p,z_i,t\right)\frac{\boldsymbol{\Phi}_\Theta\left(z_p,t\right)-\boldsymbol{\Phi}_\Theta\left(z_i,t\right)}{\left\|z_p-z_i\right\|^2}V_{ip}+ \sum_p d_{l,T}\left(z_p,z_i,t\right)\frac{T\left(z_p,t\right)-T\left(z_i,t\right)}{\left\|z_p-z_i\right\|^2}V_{ip} \tag{44}$$

where V_{ip} is the portion of the volume of layer z_p within the horizon of layer z_i.

The spatial discretization of the heat conservation Eq. (42) is:

$$\overline{(\rho C)_{av}}(z_i,t)\frac{\partial}{\partial t}\overline{T}(z_i,t)+ \rho_i\left[(C_i-C_l)(\overline{T}(z_i,t)-T_0)-L_i\right]\frac{\partial\theta_i(z_i,t)}{\partial t}= -\sum_p\lambda_s\left(z_p,z_i,t\right)\frac{T\left(z_p,t\right)-T\left(z_i,t\right)}{\left\|z_p-z_i\right\|^2}V_{ip}+ \sum_p C_l\rho_l u_l\left(z_p,z_i,t\right)\frac{\left[T\left(z_p,t\right)-T\left(z_i,t\right)\right]}{\left\|z_p-z_i\right\|}V_{ip}+ \tag{45}$$

The spatial discretization of the velocity Eq. (36) is:

$$u_l(z,t)=-\sum_{p'} d_{l,\Psi}\left(z_{p'},z_i,t\right)\frac{\boldsymbol{\Phi}_\Theta\left(z'_{p'},t\right)-\boldsymbol{\Phi}_\Theta\left(z_i,t\right)}{\left\|z_{p'}-z_i\right\|}\cdot\frac{z'_p-z_i}{\left\|z'_p-z_i\right\|}V_{ip'}- \sum_{p''} d_{l,T}\left(z_{p''},z_i,t\right)\frac{T\left(z_{p''},t\right)-T\left(z_i,t\right)}{\left\|z_{p''}-z_i\right\|}\cdot\frac{z''_p-z_i}{\left\|z''_p-z_i\right\|}V_{ip''} \tag{46}$$

where $p'\in\mathcal{H}_z^{+,\Phi}$ and $p''\in\mathcal{H}_z^{+,T}$.

The time integration is performed by the forward Euler finite difference scheme. The current state of all layers is used to calculate the change in temperature, liquid water and ice content for the next time step. The flow chart of the developed approach is presented in Fig. 3. The right part of Eq. (44) is denoted by $\Delta\Theta_l(z_i,t^n)$ and the right part of

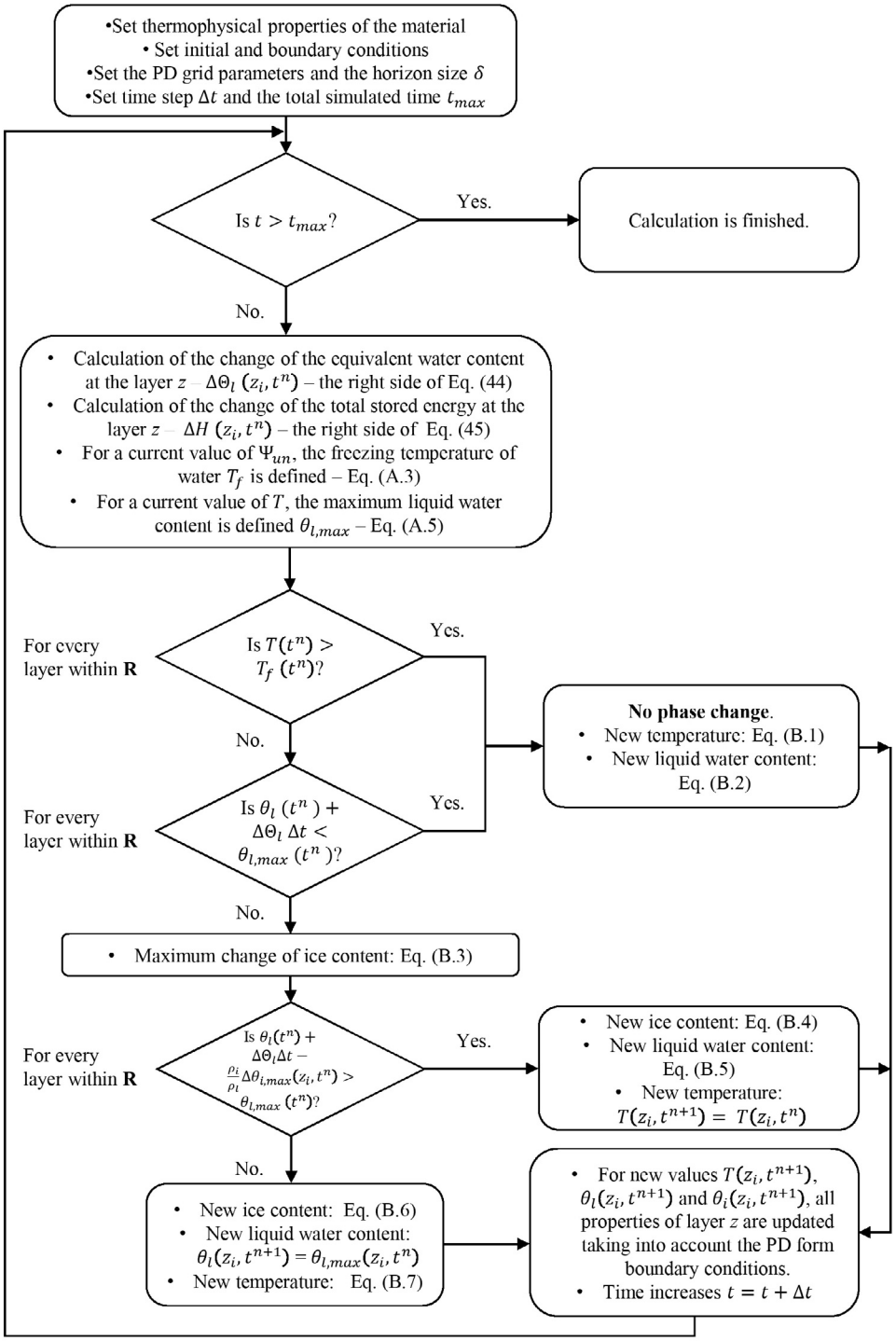

Fig. 3. The general flow-chart of the developed PD model.

Eq. (45) is denoted by $\Delta H(z_i, t^n)$. Additional equations are presented in Appendix B. This numerical scheme ensures the conservation of energy and water mass and requires relatively small computational time.

The boundary conditions are introduced by addition of several layers of boundary nodes at both sides of the considered domain. The properties of these nodes (temperature, liquid and water contents) are defined in a way that they ensure the necessary type of boundary conditions (Mei et al., 2021). It should be noted that Eq. (45) needs special attention as the water flow is governed by both soil water potential and temperature fields. However, the temperature field also defines the energy conservation within the domain (Eq. (46)). It is highly likely that the required boundary conditions for water flow and energy need different temperatures at the additional boundary nodes, e.g. the temperature of these particles must ensure zero water flux, but at the same time, it must ensure a prescribed heat flux or temperature. In these cases, the boundary particles must have two different temperatures simultaneously.

4. Model verification

To assess the accuracy of the implementation of the developed peridynamic formulations, two test problems are discussed. The calculated

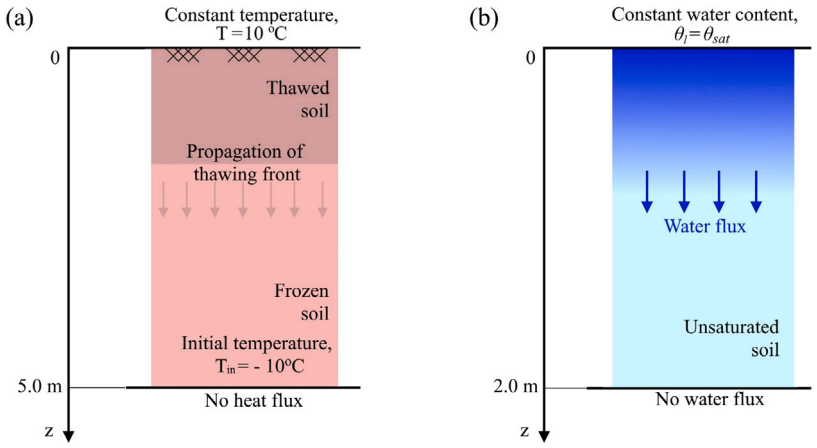

Fig. 4. Schematics of the verification problems: heat transfer in a saturated soil (a) and water transfer in an unsaturated soil (b).

results are compared with the results of analytical and finite element method (FEM) solutions for the same problems. In the first problem, heat transfer by conduction in saturated soil with phase change is simulated. In the second problem, the flow of water in unsaturated soil is considered. The finite element solution is obtained using the COMSOL Multiphysics package. The scheme of the problems are presented in Fig. 4.

The accuracy of the proposed peridynamic approach can be characterized by the global numerical error, ϵ, which can be defined as (Madenci et al., 2019; Nikolaev et al., 2023):

$$\epsilon = \frac{1}{\left|p_{\max}^{ref} - p_{\min}^{ref}\right|}\sqrt{\frac{1}{K}\sum_{n=1}^{K}\left(p_n^{ref} - p_n^{PD}\right)^2} \tag{47}$$

where p_n^{PD} and p_n^{ref} are the property of the consider soil body (e.g. temperature or water content) at the position of particle n, obtained by the solution of the PD model and by a reference method respectively, K is the total number of PD soil layers and $p_{\max}^{ref}$ and $p_{\min}^{ref}$ are the maximum and minimum absolute value of the property based on the reference calculation method.

4.1. Heat transfer by conduction with phase change

The benchmark test deals with heating a frozen soil sandy loam, which was described by Hansson et al. (2004). The thermo-physical properties of the soil are presented in Tables 2 and 3. For this problem, it is supposed that the soil is fully saturated and the densities of ice and water are equal.

The considered one-dimensional problem of heat transfer with phase change has an analytical solution (Hahn and Özisik, 2012). The problem is formulated for a semi-infinite soil domain, $0 \le z \le \infty$, with initial condition $T(z,0) = T_\infty$ and boundary conditions $T(0,t) = T_0$ (Dirichlet boundary condition) and $T(\infty,t) = T_\infty$. This solution, for the case of soil thawing, i.e. $T_0 > T_f$ and $T_\infty < T_f$, can be presented as:

$$T(z,t) = \begin{cases} T_0 + \left(T\left(z_c,t\right) - T_0\right)\dfrac{\operatorname{erf}\left(\frac{z}{(4\alpha_{un}t)^{1/2}}\right)}{\operatorname{erf}\left(\frac{\beta}{(4\alpha_{un})^{1/2}}\right)}, & 0 \le z \le z_c(t) \\ T_\infty + \left(T\left(z_c,t\right) - T_\infty\right)\dfrac{\operatorname{erfc}\left(\frac{z}{(4\alpha_f t)^{1/2}}\right)}{\operatorname{erfc}\left(\frac{\beta}{(4\alpha_f)^{1/2}}\right)}, & z_c(t) \le z \le \infty \end{cases} \tag{48}$$

where $z_c(t) = \beta\sqrt{\alpha_{un}t}$ is the position of the freezing front at time t; α_f and α_{un} are the thermal diffusivities of frozen and unfrozen soils, respectively; $\operatorname{erf}(x) = \frac{2}{\sqrt{\pi}}\int_0^x e^{-b^2}db$ is the error function; $\operatorname{erfc}(x) = 1 - \operatorname{erf}(x)$ is the complementary error function; and β is the root of the transcendental equation:

$$\frac{e^{-\beta^2}}{\operatorname{erf}(\beta)} + \frac{\Lambda_f}{\Lambda_{un}}\left(\frac{\alpha_{un}}{\alpha_f}\right)^{1/2}\frac{T\left(z_c,t\right) - T(\infty,t)}{T\left(z_c,t\right) - T(0,t)}\frac{e^{-\beta^2(\alpha_{un}/\alpha_f)}}{\operatorname{erfc}\left(\beta\sqrt{\alpha_{un}/\alpha_f}\right)} = \frac{\beta L_i\sqrt{\pi}}{C_{un}\left[T\left(z_c,t\right) - T(0,t)\right]} \tag{49}$$

where Λ_f and Λ_{un} are the heat conductivity of the frozen and unfrozen soils; C_{un} is the specific heat capacity of the unfrozen soil.

In the peridynamic model, the one-dimensional domain has a finite length of 5 m. The initial temperature of the soil is −10 °C. The top boundary has a constant temperature of +10 °C. The freezing temperature of the water is constant and equal to 0 °C. In the analytical solution, it is assumed that the water becomes frozen immediately after the phase change temperature is approached. To closely represent this condition in the peridynamic model, we assume that the liquid water content decreases linearly to the residual value as the temperature approaches −0.25 °C. The heat conductivity of the soils is defined by Eq. (A.9).

In the PD model, the time step dynamically changed and approached values up to 5 s. In the analysis, the soil domain is divided into 100, 250, 500, 1000, 2500, and 5000 peridynamic layers, corresponding to the thickness of each layer, Δ_z, ranging from $50 \cdot 10^{-3}$ to $1 \cdot 10^{-3}$ m. The relative size of the horizon, m, is chosen as 2, 3, 4, 5, 6, 8, and 10. The calculation time was 10 days.

The simulation results and their comparison with the analytical solution (48) are presented in Fig. 5 for the time instances of 1, 3 and 10 days for the layer thickness $\Delta_z = 10 \cdot 10^{-3}$ m and the horizon size $\delta = 30 \cdot 10^{-3}$. . The comparison demonstrates that there is a very good agreement between the two calculation methods.

In every calculation, the absolute numerical error is calculated at the final time instance. The value is presented in Fig. 6 for all considered layer and horizon sizes. As shown in panel (a), the value of ϵ decreases as the peridynamic layers become thinner, reaching the minimum value in the range of 0.05 to 0.1%. Further reduction is not observed due to the difference in the representation of the soil freezing characteristic curve in analytical and numerical models. The graph also shows that certain particle sizes provide minimal errors at specific values of m, for example, $\Delta_z = 20 \cdot 10^{-3}$ for $m = 3$ and $\Delta_z = 10 \cdot 10^{-3}$ for $m = 5$. This phenomenon is elucidated in panel (b), where data are presented relative to the horizon size 2δ. According to this graph, across all cases, the numerical error is minimized with a horizon size of 0.1 m. This value is specific to the model's parameters (temperature range and soil freezing curve parameters) and should not be considered universal.

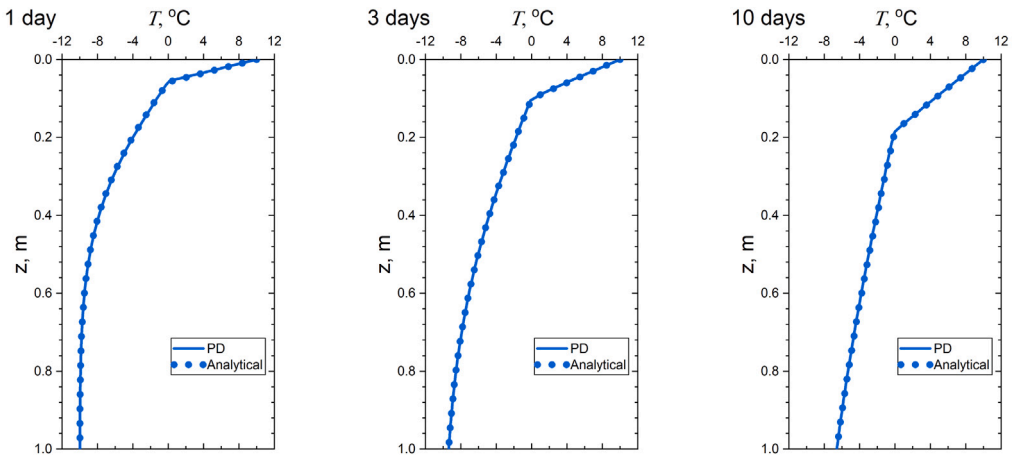

Fig. 5. The change of temperature in a saturated sandy loam at 1, 2 and 10 days time instances. The lines are the results of the developed PD model, the dots are the analytical solution, Eq. (48).

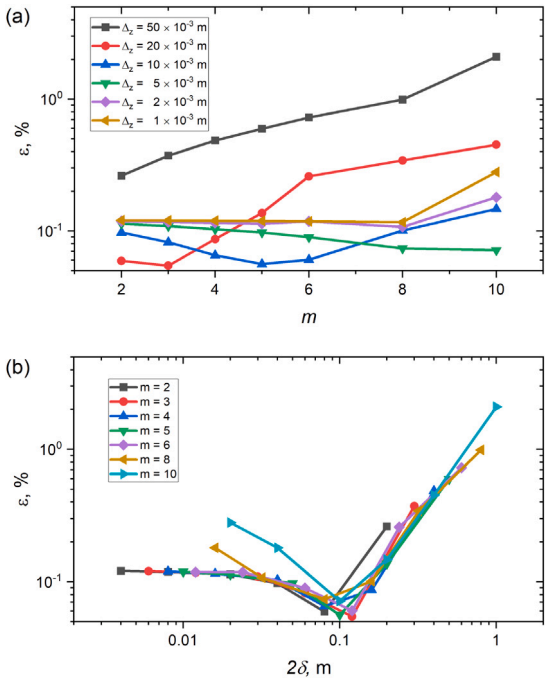

Fig. 6. Absolute numerical error ε of peridynamic solutions in the heat transfer problem with phase change that are observed for different values of m and Δ_z.

4.2. Moisture transfer in unsaturated soil

In this verification exercise, we consider the saturation of unsaturated sandy loam, which was studied in previous exercises. The results of the PD model were compared with the FEM simulation. The considered soil domain has a thickness of 2 m. Several values of the initial water content $\theta_{in,l}$ are tested: 0.3, 0.2, 0.1, as well as 0.09, 0.08, 0.07 and 0.06. As a boundary condition, a constant liquid water content is defined at the upper surface of the layer $\theta_l(z=0) = \theta_{sat} = 0.535$. The soil has a constant temperature.

In the PD model, the time step was dynamically changed and approach the values up to 5 s. In the analysis, the soils domain is divided into 40, 100, 200, 400, 1000 and 2000 soil peridynamic layers, that correspond to the thickness of each layer Δ_z from $50\cdot10^{-3}$ to $1\cdot10^{-3}$ m. The relative size of the horizon, m, is chosen as 2, 3, 4, 5, 6, 8 and 10. The calculation time was 36 h.

Fig. 7(a)–(c) presents the values of liquid water content for $\theta_{in,l}$ set to 0.3, 0.2, and 0.1 and time instances of 12, 24, and 36 h, respectively, based on PD and FEM models. These calculations are performed for a layer thickness of $\Delta_z = 10\cdot10^{-3}$ m and a horizon size of $\delta = 30\cdot10^{-3}$. For lower values of the initial water content, the applied FEM software failed to provide converged solutions due to the extremely low values of the pressure head in the unsaturated part, reaching −2982 m for the driest case. The calculation results for these low values of θ_{in} are presented in panel (d). It should be noted that to ensure the accuracy of the solution in the case of dry soils, the peridynamic calculations are performed for thinner peridynamic soil layers with $\Delta_z = 2\cdot10^{-3}$ m and a horizon size of $\delta = 6\cdot10^{-3}$.

The comparison shows that the non-local approach can achieve the same level of accuracy as the finite element method across a wide range of water content and the associated values of pore water pressure. However, in instances of very dry soils exhibiting extremely high suction values, the FEM model can struggle to converge due to the large pressure gradient within a very narrow distance range. In contrast, the developed non-local approach can handle such very dry soil conditions without encountering significant difficulties.

For the case of soils with $\theta_{in,l} = 0.3$, the absolute numerical error is calculated at the final time instance. Its value is presented for all considered peridynamic layer and horizon sizes in Fig. 8.

The results show that the accuracy of the solution increases with both the decrease in horizon size and the thickness of the soil layers. The change in horizon size can be caused by the variation in m or Δ_z. It should be noted that the difference in the error values between the solutions with the same m but different Δ_z, as seen in panel (a), is caused by the 'step-wise' shape of the resulting function of water content, Fig. 7(a). In this case, even a small variation in the predicted dynamics of the 'step' position causes the appearance of very large error values, as some of the considered soil layers adjacent to the 'step' will have a completely different water content.

The presented verification exercises prove the accuracy of the developed numerical procedure. In the next section, this model is applied to describe the behaviour of various types of soils.

5. Validation and application

Four validation exercises are performed to demonstrate the ability of the proposed PD formulation to reproduce experimentally observed behaviours. The selected experiments are: Mizoguchi (1990) experiment of freezing sandy loam; Watanabe et al. (2013) experiment of freezing silty loam; Zhou et al. (2014) experiment of freezing loamy silt; and Jame and Norum (1980) experiment of freezing silica flour. These have been used to validate various numerical models based on

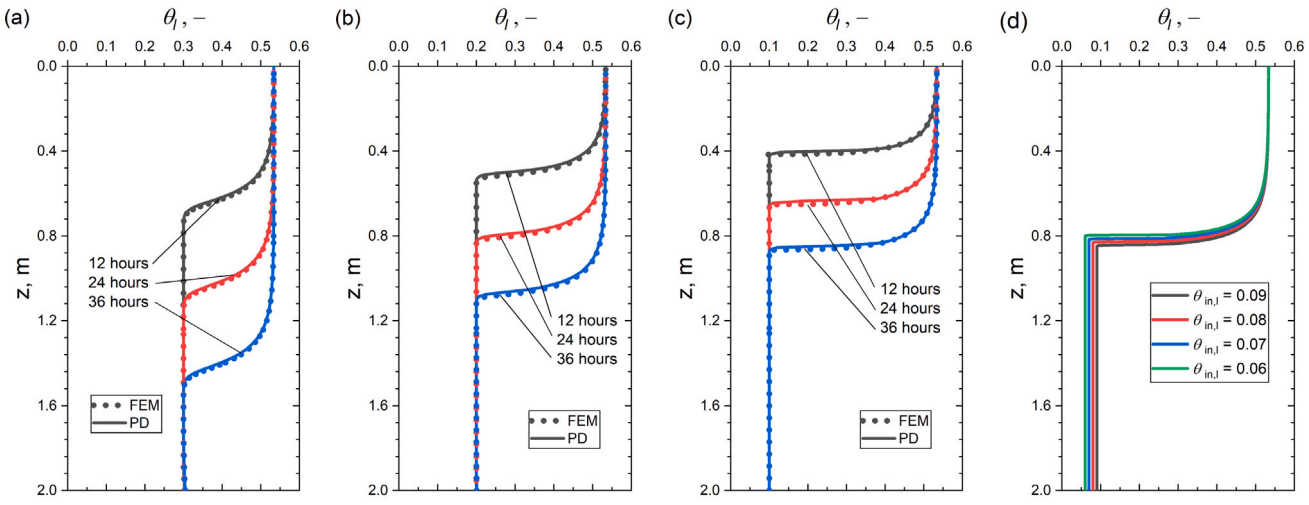

Fig. 7. The change of liquid water content in the unsaturated sandy loam at 12, 24 and 36 h time instances (panels (a) – (c)) and at the time instance 36 h (panel (d)). The lines are the results of the developed PD model, the dots are the results of the FEM simulation.

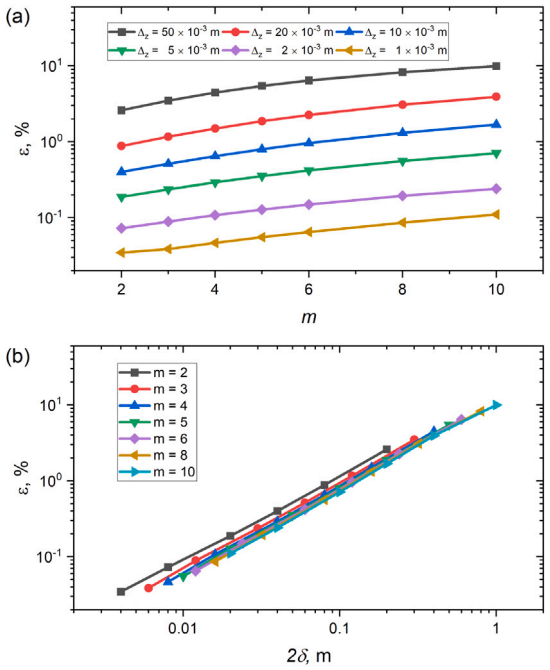

Fig. 8. Absolute numerical error ϵ of peridynamic solutions in the problem of water transfer in unsaturated soils that are observed for different values of m and Δ_z.

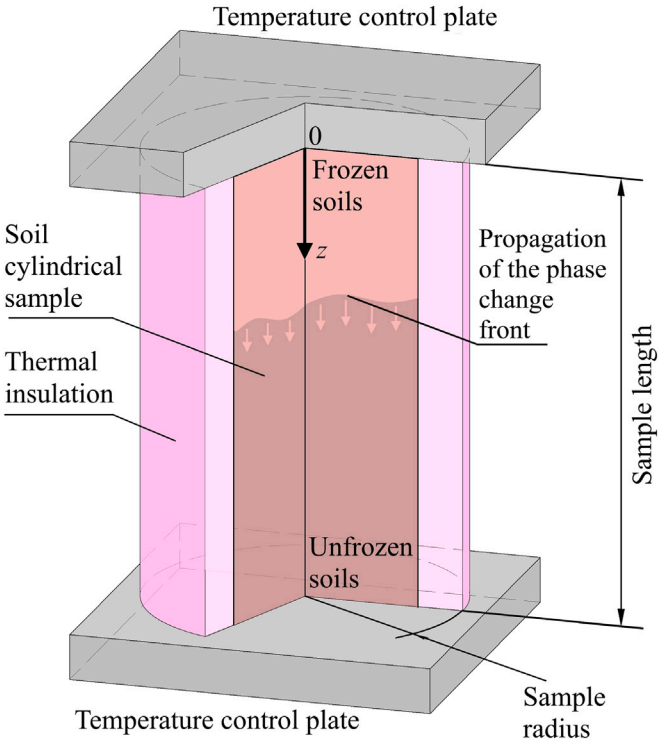

Fig. 9. The scheme of 1D experiments of soil freezing.

FEM and other numerical methods. General information about these experiments, as well as a comprehensive list of numerical studies where they have been used, is presented in Table 1. They have similar set-ups: a vertical or a horizontal soil cylinder with known physical properties and water content was exposed to a low temperature from one side, whereas the boundary of the soil column froze and the freezing front propagated along the cylinder. A conceptual diagram of the set-up is shown in Fig. 9.

5.1. Freezing of Kanagawa sandy loam

The description and the results of the laboratory study (Mizoguchi, 1990) were presented in Hansson et al. (2004). Four vertical cylinders of Kanagawa sandy loam with a length of 20 cm and a diameter of 8 cm were used. The initial water content in all cylinders was $\theta_{in,l}$ = 0.335. The cylinders had initial (nearly) uniform temperature of 6.7 °C and were subsequently cooled from above by a flowing liquid with unknown properties so that −6 °C was reached and maintained at the top surface. The cooling of the cylinders was interrupted after 12, 24 and 50 h, and the samples were sliced to measure the water content.

The modelling of this experimental procedure requires convective heat flux to be prescribed as a boundary condition (Hansson et al., 2004; Liu and Yu, 2011). However, the convective heat transfer coefficient is unknown, and in the present study it is assumed to be 25 W/(m^{2}K). The thermal conductivity of soil is defined by Eq. (A.10). Other properties of the soil are presented in Tables 2 and 3. The impedance factor, Eq. (A.7), is assumed to be η = 10. The time step

Table 1
General information about considered laboratory experiments.

Experiment details	Mizoguchi (1990), Hansson et al. (2004)	Watanabe et al. (2013)	Zhou et al. (2014)	Jame and Norum (1980)
Type of soils	Sandy loam	Silty loam	Loamy silt	Silica flour
Soil sample	20 cm vertical cylinder with ⌀ 8 cm	35 cm vertical cylinder with ⌀ 7.8 cm	23.6 cm vertical cylinder with ⌀ 5.3 cm	30 cm horizontal cylinder with ⌀ 10 cm
Duration of experiment	50 h	50 h	72 h	72 h
Thermal BC (top / bottom, or left / right)	convective heat flux / zero heat flux	constant temperature / constant temperature	convective heat flux / zero heat flux	constant temperature / constant temperature
Hydraulic BC (top / bottom, or left / right)	zero water flux / zero water flux	zero water flux / zero water flux	zero water flux / zero water flux	zero water flux / zero water flux
Studies discuss the experiment	Painter (2011), Painter and Karra (2014), Peng et al. (2016), Zhang et al. (2016b), Li et al. (2021), Stuurop et al. (2021)	Stuurop et al. (2021)	Stuurop et al. (2021), Chen et al. (2022)	Painter (2011), Painter and Karra (2014), Peng et al. (2016), Zhou and Zhou (2010), Liu and Yu (2011), Sheshukov and Nieber (2011), Karra et al. (2014), Chen et al. (2022), Fu et al. (2023)

Table 2
Parameters of the model test problems.

Properties	Sandy loam (Mizoguchi, 1990)	Silt loam (Watanabe et al., 2013)	Silt loam (Zhou et al., 2014)	Silica flour (Jame and Norum, 1980)
$\epsilon = \theta_{sat}$, [−]	0.535	0.617	0.467	0.5
θ_{res}, [−]	0.05	0.006	0.05	0.005
K_{sat}, [ms^{-1}]	3.2 $\cdot 10^{-6}$	2.1 $\cdot 10^{-6}$	0.3 $\cdot 10^{-6}$	2.0 $\cdot 10^{-6}$
α_{vg}, [m^{-1}]	1.11	0.88	0.11	0.31
n_{vg}, [−]	1.48	1.25	2.2	3
Λ_s, [Wm^{-1}K^{-1}]	0.55	0.4	1	2

Table 3
Thermophysical properties of the soil components.

Λ_l, [Wm^{-1}K^{-1}]	0.6
Λ_i, [Wm^{-1}K^{-1}]	2.14
Λ_a, [Wm^{-1}K^{-1}]	0.025
C_s, [J kg^{-1}K^{-1}]	840
C_l, [J kg^{-1}K^{-1}]	4182
C_i, [J kg^{-1}K^{-1}]	2180
C_a, [J kg^{-1}K^{-1}]	1000
ρ_s, [kg m^{-3}]	2648
ρ_l, [kg m^{-3}]	1000
ρ_i, [kg m^{-3}]	916
ρ_a, [kg m^{-3}]	1.28
L_f, [kJ kg^{-1}]	334

in the PD simulations was 0.25 s. The layer thickness was $2 \cdot 10^{-3}$ m and the PD horizon was $6 \cdot 10^{-3}$m.

The simulation results are presented in Fig. 10 together with the experimental results. Close agreement between the two can be observed. The position of the phase change front and the water content in the unfrozen and frozen parts are accurately predicted by the model. A slight disagreement between numerical and experimental results is observed at the top boundary of the cylinders ($z = 0$), where the predicted total water content is lower than the experimental one. It can be explained by the specificity of the developed PD approach. Here, Eq. (28) is used to define the hydraulic conductivity of t-bonds, and therefore the hydraulic conductivity of the horizon drops when its centre has nearly zero conductivity. When the temperature of the upper PD layer of the model becomes negative and the conductivity becomes nearly zero, the inflow to this layer is prevented. As a result, the total water content of the layers adjacent to the top boundary remains nearly equal to the initial value.

It should be noted, that results of the developed PD approach are in better agreement with the experimental data than the models proposed in Hansson et al. (2004) and Dall'Amico et al. (2011), and are in similar agreement as the models developed in Stuurop et al. (2021).

It should be also noted that in contrast to the other experiments considered in this study, the Mizoguchi experiment sets a constant temperature only on one side of the cylinder. In such case, the freezing front steadily propagates through the cylinder, and if the experiment has not been stopped at 50 h, the entire body would have frozen after some time. Therefore, there is no significant water accumulation at any cross-section, which could happen if the propagation of the phase change front stops due to reaching temperature steady-state conditions.

To assess the influence of domain discretization, calculations were conducted for various numbers of peridynamic layers: 20, 40, 80, 100, 120, 160, and 320, corresponding to the layer thickness Δ_z ranging from 10^{-2} to $6.25 \cdot 10^{-4}$ m. During the calculations, the total water content Θ_w was determined. The calculation results for horizontal cross sections with positions z at 0.05, 0.1, and 0.15 are presented in Fig. 11.

The results show that the solution is not discretization-independent. With the decrease in particle size, the values of the total water content converge to some values that can be considered as the true solution. However, as seen, only very thick peridynamic soil layers compromise accuracy significantly. After approaching a critical size, the influence of this parameter on the solution becomes insignificant.

It is noted that thicker peridynamic layers are more suitable for practical applications in which calculation domains have large sizes. It significantly reduces the computational time because the total number of domain division in the model becomes smaller, and, moreover, solving the problem with larger particles can be performed with a larger time step. Therefore, in this section, for all validation problems, we focus on a domain discretization in which the particle size is chosen as one of the largest possible thicknesses that ensure solution accuracy.

5.2. Freezing of silt loam from Tokachi District, Hokkaido

The soil used in the laboratory experiment by Watanabe et al. (2013) was a silty loam. The soil samples were packed in cylinders with a diameter of 7.8 cm and a height of 35 cm. These cylinders were vertically placed between two temperature-controlled plates, the top one had a temperature of −6.2 °C and the bottom one a temperature of 2 °C. Three experiments with initial liquid water contents of 0.31, 0.38 and 0.46, were performed. Other thermo-physical properties are presented in Tables 2 and 3. In the PD model, the time step was 0.25 s. The layer thickness was $3.5 \cdot 10^{-3}$ m and the PD horizon was $9.5 \cdot 10^{-3}$m. The impedance factor in Eq. (A.7) was assumed to be $\eta = 10$. The heat conductivity of the soils is defined by Eq. (A.9).

The simulation and experimental results are shown in Fig. 12, where a very good agreement can be observed. The thermal conductivity of the solid grains and their density was not presented in Watanabe et al. (2013), and was applied according to Stuurop et al. (2021). A more

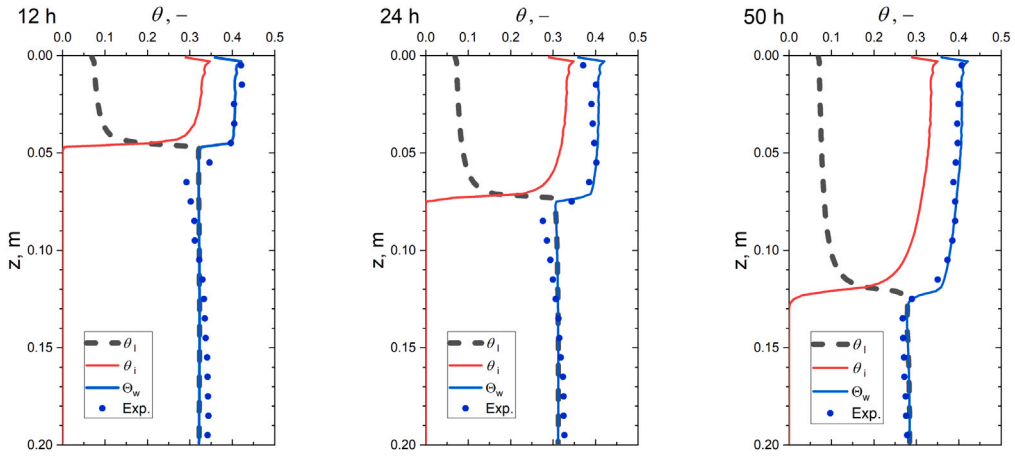

Fig. 10. The change of total water content in a sandy loam cylinder at 12, 24 and 50 h time instances. The lines are the results of the developed PD model, the dots are the results of the experimenter (Mizoguchi, 1990) (based on Hansson et al. (2004)).

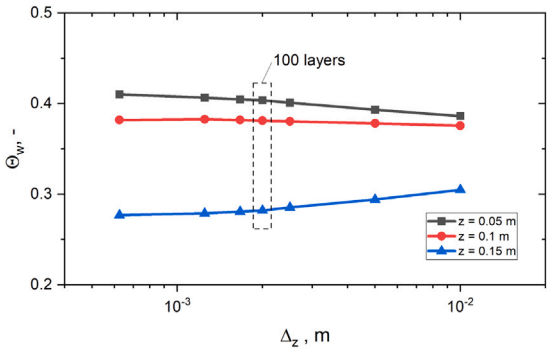

Fig. 11. Variations of the total water content Θ_w for three soil sample cross sections depending on the thickness of the peridynamic layer Δ_z.

Table 4
Experimental conditions for 4 experiments (Zhou et al., 2014).

	1 exp.	2 exp.	3 exp.	4 exp.
Initial water content, –	0.325	0.160	0.225	0.167
Top temperature, [°C]	−4	−4.7	−4.2	−2.1
Bottom temperature, [°C]	3.6	3.5	4.1	3.8

Table 5
Experimental conditions for 3 experiments (Jame and Norum, 1980).

	1 exp.	2 exp.	3 exp.
Initial water content, –	0.156	0.15	0.101
Left temperature, [°C]	−10	−5.5	−5.3
Right temperature, [°C]	20	4.5	5

accurate assessment of these parameters can improve the agreement. For example, it was proposed to change the parameter n_{vg} to increase the agreement between calculation and laboratory data (Stuurop et al., 2021). This can indeed improve the agreement for the case with initial $\theta_l = 0.38$, however, for the two other cases the accuracy decreases. Therefore, this value was not modified here, but selected based on Watanabe et al. (2013).

5.3. Freezing of silt loam from Turtmann valley, Switzerland

The behaviour of silty loam was studied by an extensive set of laboratory experiments (Zhou et al., 2014). Four separate experiments were conducted. Vertical soil cylinders with 0.053 m inner diameter and 0.236 m length were frozen from their top surfaces in 72 h time intervals. During the test, the liquid and ice contents, and also the change in temperature profiles were measured. The thermophysical properties of the soils are presented in Tables 2 and 3. The conditions of the experiments are presented in Table 4. It should be noted that according to the data, presented in Zhou et al. (2014), the temperature at the top boundary was not constant. It was higher at the initial stage, and only after certain time, it decreased to the reported values. Therefore, in the numeric simulation, the convective boundary condition is applied at the top boundary with a convective heat transfer coefficient of 400 $W/(m^2K)$. In the PD model, the time step was 0.25 s. The layer thickness was $2.35 \cdot 10^{-3}$ m and the PD horizon was $7.05 \cdot 10^{-3}$ m. The impedance factor in Eq. (A.7) was assumed to be $\eta = 9$. The heat conductivity of the soils is defined by Eq. (A.9).

The results presented in Fig. 13, show a good agreement between the experimental data and the calculated behaviour for the first and fourth experiments, even if the PD model predicts the narrower transition area between frozen and unfrozen zones. However, laboratory experiments 2 and 3 cannot be reproduced by the model with the same values of the soil properties. Even when the position of the phase change front and its dynamics are captured well, a significant amount of water accumulates around the steady-state position of the freezing front, more than can be mathematically predicted. It is noted that by the end of the experiments, the steady-state temperature fields were almost reached. When this happens, the velocity of the phase change front significantly decreases, which gives the pore water more time to flow to the front and accumulate there. It is clearly observed in the results for all cases except the one with $\theta_l = 0.325$.

5.4. Freezing of silica flour

The experiments reported in Jame and Norum (1980) used horizontal cylindrical soil samples with a height of 0.3 m and a diameter of 0.1 m. The left and right boundaries of the sample had a constant temperature. There is no information about the thermo-physical and hydraulic properties of the soil that can be used in the simulation. Therefore, all model parameters were defined based on information from other papers. The parameters used are presented in Tables 2 and 3. There were three sets of experiments with different initial water content and boundary temperatures. The total time of all experiments was 72 h. Information about the experimental conditions is presented in Table 5. The thermal conductivity of the soil is defined by Eq. (A.10). In the PD model, the time step was 0.15 s. The layer thickness was $3 \cdot 10^{-3}$ m and the PD horizon is $9 \cdot 10^{-3}$m.

The computational results and corresponding experimental data are presented in Fig. 14. The comparison shows that the developed model

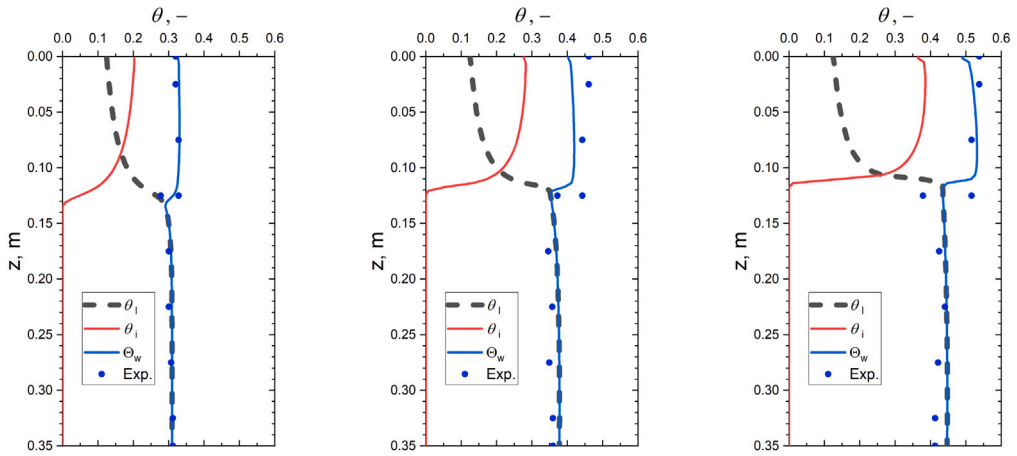

Fig. 12. The change of total water content in silt loam cylinders with different initial water content $\theta_{l,in}$ after 50 h of freezing. The lines are the results of the developed PD model, and the dots are the results of the experimenter (Watanabe et al., 2013).

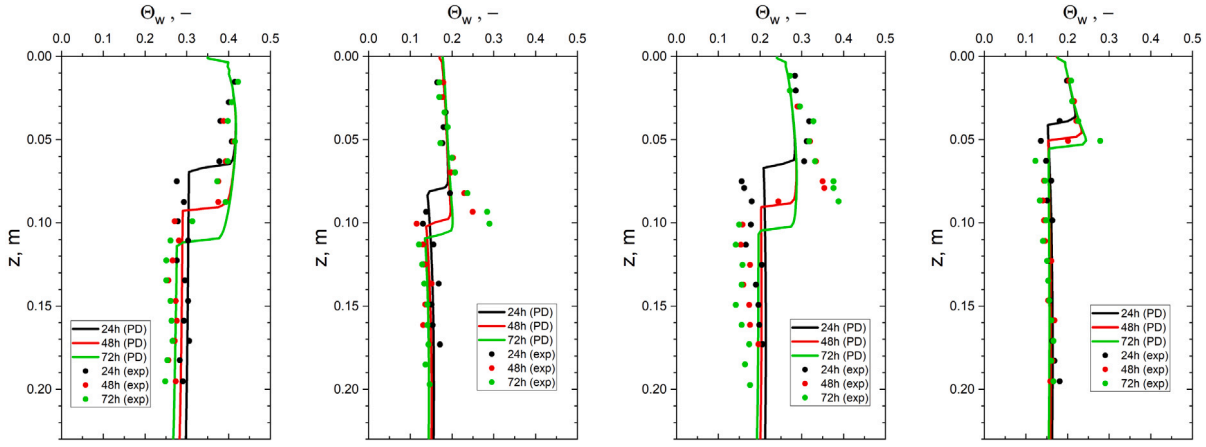

Fig. 13. The change of total water content in a silt loam cylinder with different initial water content $\theta_{l,in}$. The lines are the results of the developed PD model, and the dots are the results of the experimenter (Zhou et al., 2014).

can describe well heat and water transfer in freezing soils. There is a very good agreement for the first test between the experimental data and the simulations for the frozen part of the sample during the entire experiment time. However, the predicted total water content in the unfrozen part is higher. Such behaviour cannot be reasonably explained in the framework of the existing theories. It should be noted, that in the study (Peng et al., 2016), only the second and third tests were considered, possibly because of the above observation. A better agreement for the unfrozen zone in the first test was demonstrated in Painter (2011), Painter and Karra (2014) and Karra et al. (2014). However, in all their attempts, the authors overpredicted the water content in the frozen zone, especially in the region close to the cold end of the sample. It is, therefore, possible that for the first test, conservation of water mass was not maintained in the laboratory experiment, possibly due to a high evaporation rate during the long 72 h experiment in the presence of a source of relatively high temperature (+ 20 ℃).

It should be noted that even if the temperature at the left (cold) boundary was nearly constant during the experiment, during the first 4 h, it was sufficiently higher. Because of this, a slight disagreement between experimental and simulation results is observed in the initial times.

6. Conclusions

The paper presents a rigorous mathematical derivation of the general forms of heat and mass conservation equations that describe the behaviour of frozen unsaturated soils. The heat conservation equation considers the effective latent heat of solidification. The mass conservation equation takes into account the moisture transfer due to isothermal and thermal mass liquid diffusivity, and is derived to consider the coexistence of liquid and solid water in pores at negative temperatures. These general forms of conservation equations can become a foundation for developing local and non-local analytical and numerical models.

A new non-local coupled model for calculating the temperature change and liquid transfer in unsaturated frozen soils was developed and presented within the framework of bond-based Peridynamic theory. The model was shown to reproduce the results of several laboratory experiments with good agreement, except in some rather anomalous cases discussed in the paper.

The proposed model is the first Peridynamic formulation of diffusion equations that combines the water mass transfer defined by isothermal and non-isothermal liquid conductivity with heat transfer and change of water state. It was demonstrated that for the soils with relatively high initial water content, the developed approach effectively captured the change of liquid water content.

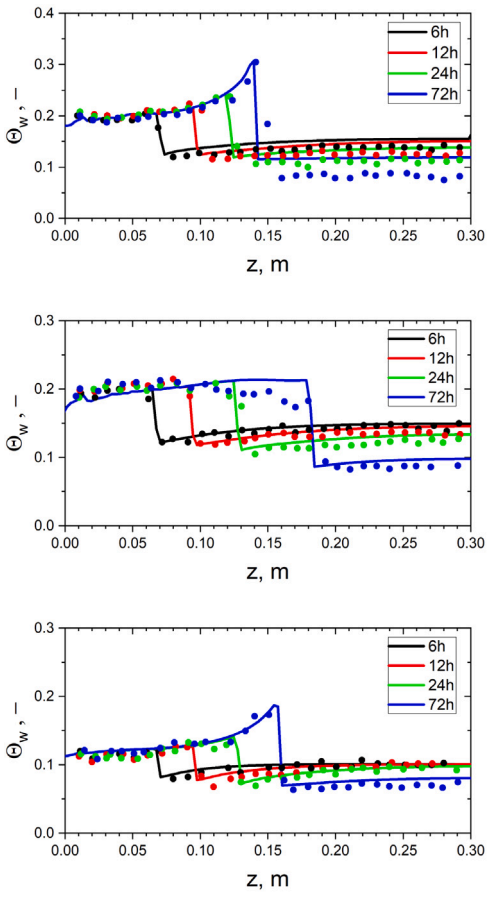

Fig. 14. The change of total water content in a silica flour Θ_w. The lines are the results of the developed PD model, the dots are the results of the experimenter (Jame and Norum, 1980).

The set of integral–differential peridynamic equations is solved by a simple numerical scheme. The developed non-local approach can be used as a basis for the development of a fully coupled physically based model of frost heave.

CRediT authorship contribution statement

Petr Nikolaev: Conceptualization, Data curation, Formal analysis, Investigation, Methodology, Software, Validation, Visualization, Writing – original draft, Writing – review & editing. **Andrey P. Jivkov:** Conceptualization, Methodology, Supervision, Writing – original draft, Writing – review & editing. **Lee Margetts:** Conceptualization, Methodology, Supervision, Writing – original draft, Writing – review & editing. **Majid Sedighi:** Conceptualization, Methodology, Supervision, Writing – original draft, Writing – review & editing.

Declaration of competing interest

The authors declare that they have no known competing financial interests or personal relationships that could have appeared to influence the work reported in this paper.

Data availability

Data will be made available on request.

Acknowledgements

The financial support received by P. Nikolaev in the form of a President doctoral scholarship award (PDS award) by the University of Manchester is gratefully acknowledged. A.P. Jivkov and L. Margetts are grateful for the financial support of the Engineering and Physical Sciences Research Council, UK (EPSRC) via grant EP/N026136/1. The authors would like to acknowledge the assistance given by Research IT and the use of the Computational Shared Facility at The University of Manchester.

Appendix A. Hydraulic and thermal properties of frozen soils

According to the semi-empirical approach presented in Stuurop et al. (2021), see also Dall'Amico et al. (2011), Painter and Karra (2014) and Chen et al. (2022), the soil pore water potential includes the terms that can be defined by the Clausius–Clapeyron equation and van Genuchten model. The soil water potential, as a function of the total water content, is described by the van Genuchten (1980) relationship:

$$\Psi_\Theta = -\frac{1}{a_{vg}}\left[\left(\frac{\theta_{sat}-\theta_{res}}{\Theta_w-\theta_{res}}\right)^{\frac{n_{vg}}{n_{vg}}-1}-1\right]^{\frac{1}{n_{vg}}} \tag{A.1}$$

The soil water potential associated with the coexistence of liquid and solid water at negative temperatures and governed by the Clausius–Clapeyron equation is:

$$\Psi_T = \begin{cases} \frac{L_i}{gT_f}(T-T_f), & \text{if} \quad T < T_f \\ 0, & \text{if} \quad T \geq T_f \end{cases} \tag{A.2}$$

where θ_{sat} is the saturated volumetric water content $[\mathrm{m}^3/\mathrm{m}^3]$; θ_{res} is the residual total water content $[\mathrm{m}^3/\mathrm{m}^3]$; a_{vg}, $[1/m]$, and n_{vg}, $[-]$ are the van Genutchten parameters, that depend on the type of soils.

Following Dall'Amico et al. (2011), the initial temperature of water solidification T_f can be defined according to the Clausius–Clapeyron equation as:

$$T_f = T_0 + \frac{gT_0}{L}\Psi_\Theta \tag{A.3}$$

The surface tension of water, σ, which is required for calculating the modified thermal mass liquid diffusivity for frozen and unfrozen conditions by Eq. (13), can be described as discussed in Saito et al. (2006).:

$$\sigma = \left(75.6 - 0.1425T - 0.000238T^2\right)10^{-3} \tag{A.4}$$

where T is temperature in °C.

As indicated in Painter and Karra (2014), the maximum temperate at which the ice can exist (or, the freezing temperature of water) is lower for water within soils than in its bulk state. With the increase of gas content in soils, the freezing temperature depression also decreases, which was indicated e.g., by Kozlowski (2004). According to the experimental study (Zhou et al., 2014), when the equilibrium water content is higher than the unfrozen water content for a given temperature $T < T_f$, its value should be described by the soil water potential. If they are equal, θ_l depends only on the temperature and can be described by the Clausius–Clapeyron equation. Following this conclusion, the physical approach, discussed in Stuurop et al. (2021), can be modified to derive an approximation for the soil freezing curve that defines the maximum unfrozen water content in frozen soils $\theta_{l,max}$ at a given temperature $T < T_f$. In this case, the modification of the relation proposed in Zheng et al. (2021) can be used, see also (Zhang et al., 2016b), which is derived by the introduction of Eq. (9) to the van Genuchten (1980) model as:

$$\theta_{l,max} = \theta_{l,res} + \frac{\left(\theta_{l,sat}-\theta_{l,res}\right)}{\left(\left|a_{vg}\Psi\right|^{n_{vg}}+1\right)^{\frac{n_{vg}-1}{n_{vg}}}} \tag{A.5}$$

It should be noted, that in Zhang et al. (2016b) and Zheng et al. (2021), instead of the term Ψ, the value Ψ_T was used. Taking into account Ψ_Θ, as a part of Ψ, ensures the dependence of liquid water content on its initial value.

The unsaturated hydraulic conductivity of frozen and unfrozen soils can be described by the same relation. In this case, the classical van Genuchten relation can be used:

$$K_l = K_{l_s at}\left(\frac{\theta_l-\theta_{res}}{\theta_{sat}-\theta_{res}}\right)^{1/2}\left\{1-\left[1-\left(\frac{\theta_l-\theta_{res}}{\theta_{sat}-\theta_{res}}\right)^{\frac{n_{vg}}{n_{vg}-1}}\right]^{\frac{n_{vg}-1}{n_{vg}}}\right\}^2 \tag{A.6}$$

where $K_{l_s at}$ is the saturated hydraulic conductivity, [m/s].

When the water became frozen, the liquid water content drops, which leads to a significant decrease in hydraulic conductivity defined according to Eq. (A.6). However, this decrease is not high enough, as was indicated in, e.g. Stuurop et al. (2021), therefore it is generally suggested that the value K_l should be additionally multiplied by, the so-called, impedance factor I, which will further decrease the hydraulic conductivity, when the ice appears and blocks the porous flow. The following empirical relation can be used:

$$I = 10^{-\eta\frac{\theta_i}{\theta_w}} \tag{A.7}$$

where η is an empirical shape parameter.

It should be noted that the introduction of impedance factor to the numerical models is widely criticized as it can be considered as a purely arbitrary correction function that is used to reach correspondence between the experimental and simulation data. In Newman and Wilson (1997) and Watanabe and Wake (2009), it was stated that the presence of impedance factor is unnecessary if the soil water retention curve and soil freezing characteristic curve are defined accurately. Due to that, some modern mathematical models, see e.g. Painter (2011) and Zhang et al. (2016c), do not take the impedance factor into account. However, in the present study, this parameter is taken into account, as the accurate forms of these soil characteristics are not available very often. Moreover, even if these functions can be assessed by studying soil samples in the laboratory, these relationships may not correspond to the relations for the undisturbed soils in their natural state.

The total heat content H in a unit volume of soil region $\mathcal{B}$, neglecting the effect of differential heat of wetting, can be defined as:

$$\begin{aligned} H =& \rho_i C_i \theta_i (T-T_0) - \rho_l C_l \theta_l (T-T_0) + \\ & \rho_s C_s (1-\epsilon)(T-T_0) + \rho_a \theta_a C_a (T-T_0) + L_i \rho_l \theta_l, \end{aligned} \tag{A.8}$$

where C_n denote the specific heat capacities of different phases; T_0 is the reference temperature, [K], taken to be equal to the freezing temperature of pure water.

A number of models for Λ_{av} have been proposed, however, their accuracy is quite low (He et al., 2020a, 2021). In the present study, the thermal conductivity of unsaturated soils is defined differently:

– as a geometric average (Zhang et al., 2016c; Zhou et al., 2022):

$$\Lambda_{av} = \Lambda_l^{\theta_l}\Lambda_i^{\theta_i}\Lambda_s^{(1-\epsilon)}\Lambda_a^{\theta_a} \tag{A.9}$$

– as a simple (arithmetic) average (Amiri et al., 2018; Stuurop et al., 2021):

$$\Lambda_{av} = \Lambda_l\theta_l + \Lambda_i\theta_i + \Lambda_s(1-\epsilon) + \Lambda_a\theta_a \tag{A.10}$$

where $\Lambda_l, \Lambda_i, \Lambda_s$ and Λ_a are the thermal conductivity of liquid water, ice, soil grains and air, [W/(mK)], respectively. These and other forms of the analytical determination of soil heat conductivity were discussed in Dong et al. (2015). It was mentioned that Eq. (A.9) is more accurate for soils with higher water content; however, as saturation approaches, the heat conductivity is overestimated. For small water content, the method could underestimate the conductivity. Eq. (A.10) generally overestimates Λ_{av} regardless of the water content. However, no reliable method was proposed to choose which method is more suitable for particular soils. Therefore, in Section 5, the calculation method is defined empirically to ensure the best possible representation of the dynamics of the phase front.

Appendix B. Details of numerical implementation

In this Appendix, supplementary relationships to the numerical representation of the model that is described by the flow chart (Fig. 3) are presented.

$$T\left(z_i, t^{n+1}\right) = T(z_i, t^n) + \frac{\Delta H(z_i,\ t^n)}{\overline{(\rho C)}_{av}(z_i,t)}\Delta t \tag{B.1}$$

$$\theta_l\left(z_i, t^{n+1}\right) = \theta_l\left(z_i, t^n\right) + \Delta\Theta_l\left(z_i, t^n\right)\Delta t \tag{B.2}$$

$$\Delta\theta_{l,max}(z_i, t^n) = \frac{\Delta H(z_i, t^n)\Delta t}{\rho_i(C_i - C_l)\left[T(z_i,t^n) - T_f(z_i,t^n)\right] - \rho_i L_i} \tag{B.3}$$

$$\theta_i(z_i, t^{n+1}) = \theta_i(z_i, t^n) + \Delta\theta_{i,max}(z_i, t^n) \tag{B.4}$$

$$\theta_l(z_i, t^{n+1}) = \theta_l(z_i, t^n) + \Delta\Theta_l(z_i, t^n)\Delta t - \frac{\rho_i}{\rho_l}\Delta\theta_{i,max}(z_i, t^n) \tag{B.5}$$

$$\theta_i(z_i, t^{n+1}) = \theta_i(z_i, t^n) + \frac{\rho_i}{\rho_l}\left[\theta_l(z_i, t^n) + \Delta\Theta_l(z_i, t^n)\Delta t - \theta_{l,max}(z_i, t^n)\right] \tag{B.6}$$

$$\begin{aligned} T(z_i, t^n) =& T(z_i, t^n) + \frac{\Delta H(z_i, t^n)\Delta t}{\overline{(\rho C)}_{av}(z_i, t)} \\ & - \left(\rho_i(C_i - C_l)\left[T(z_i,t^n) - T_f(z_i,t^n)\right] - \rho_i L_i\right)\left(\theta_i(z_i,t^{n+1}) - \theta_i(z_i,t^n)\right) \end{aligned} \tag{B.7}$$

References

Amiri, E.A., Craig, J.R., Kurylyk, B.L., 2018. A theoretical extension of the soil freezing curve paradigm. Adv. Water Resour. 111, 319–328. http://dx.doi.org/10.1016/j.advwatres.2017.11.021.

Bai, R., Lai, Y., Zhang, M., Ren, J., 2020. Study on the coupled heat-water-vapor-mechanics process of unsaturated soils. J. Hydrol. 585, 124784. http://dx.doi.org/10.1016/j.jhydrol.2020.124784.

Bobaru, F., Duangpanya, M., 2010. The peridynamic formulation for transient heat conduction. Int. J. Heat Mass Transfer 53 (19–20), 4047–4059. http://dx.doi.org/10.1016/j.ijheatmasstransfer.2010.05.024.

Bobaru, F., Duangpanya, M., 2012. A peridynamic formulation for transient heat conduction in bodies with evolving discontinuities. J. Comput. Phys. 231 (7), 2764–2785. http://dx.doi.org/10.1016/j.jcp.2011.12.017.

Chen, Z., Bobaru, F., 2015. Selecting the kernel in a peridynamic formulation: A study for transient heat diffusion. Comput. Phys. Comm. 197, 51–60. http://dx.doi.org/10.1016/j.cpc.2015.08.006.

Chen, W., Gu, X., Zhang, Q., Xia, X., 2021. A refined thermo-mechanical fully coupled peridynamics with application to concrete cracking. Eng. Fract. Mech. 242, 107463. http://dx.doi.org/10.1016/j.engfracmech.2020.107463.

Chen, Y., Lai, Y., Li, H., Pei, W., 2022. Finite element analysis of heat and mass transfer in unsaturated freezing soils: Formulation and verification. Comput. Geotech. 149, 104848. http://dx.doi.org/10.1016/j.compgeo.2022.104848.

Dall'Amico, M., Endrizzi, S., Gruber, S., Rigon, R., 2011. A robust and energy-conserving model of freezing variably-saturated soil. Cryosphere 5 (2), 469–484. http://dx.doi.org/10.5194/tc-5-469-2011.

Dong, Y., McCartney, J.S., Lu, N., 2015. Critical review of thermal conductivity models for unsaturated soils. Geotech. Geol. Eng. 33 (2), 207–221. http://dx.doi.org/10.1007/s10706-015-9843-2.

Fu, H., Song, E., Tong, R., 2023. A numerical model for hydrothermal transport in unsaturated freezing soils considering thermodynamics equilibrium. Int. J. Numer. Anal. Methods Geomech. nag.3490. http://dx.doi.org/10.1002/nag.3490.

Güémez, J., Fiolhais, C., Fiolhais, M., 2001. Reproducing Black's experiments: freezing point depression and supercooling of water. Eur. J. Phys. 23 (1), 83.

Hahn, D.W., Özisik, M.N., 2012. Heat Conduction, third ed. John Wiley & Sons, Inc., p. 718.

Hansson, K., Šimůnek, J., Mizoguchi, M., Lundin, L.-C., van Genuchten, M.T., 2004. Water flow and heat transport in frozen soil: Numerical solution and Freeze–Thaw applications. Vadose Zone J. 3 (2), 693–704. http://dx.doi.org/10.2136/vzj2004.0693.

He, H., Flerchinger, G.N., Kojima, Y., Dyck, M., Lv, J., 2021. A review and evaluation of 39 thermal conductivity models for frozen soils. Geoderma 382, 114694. http://dx.doi.org/10.1016/j.geoderma.2020.114694.

He, H., Noborio, K., Johansen, O., Dyck, M.F., Lv, J., 2020a. Normalized concept for modelling effective soil thermal conductivity from dryness to saturation. Eur. J. Soil Sci. 71 (1), 27–43. http://dx.doi.org/10.1111/ejss.12820.

He, Z., Teng, J., Yang, Z., Liang, L., Li, H., Zhang, S., 2020b. An analysis of vapour transfer in unsaturated freezing soils. Cold Reg. Sci. & Technol. 169, 102914. http://dx.doi.org/10.1016/j.coldregions.2019.102914.

He, Z., Zhang, S., Teng, J., Yao, Y., Sheng, D., 2018. A coupled model for liquid water-vapor-heat migration in freezing soils. Cold Reg. Sci. & Technol. 148, 22–28. http://dx.doi.org/10.1016/j.coldregions.2018.01.003.

Hou, B., Jin, H., Flerchinger, G., Lv, J., He, H., 2023. Canopy effect: water vapor transmission in frozen soils with impermeable surface. Acta Geotech. 18 (10), 5385–5401. http://dx.doi.org/10.1007/s11440-023-01845-0.

Huang, X., Rudolph, D.L., 2023. Numerical study of coupled water and vapor flow, heat transfer, and solute transport in variably-saturated deformable soil during freeze-thaw cycles. Water Resour. Res. 59 (10), e2022WR032146. http://dx.doi.org/10.1029/2022WR032146.

Jabakhanji, R., Mohtar, R.H., 2015. A peridynamic model of flow in porous media. Adv. Water Resour. 78 (January), 22–35. http://dx.doi.org/10.1016/j.advwatres.2015.01.014.

Jafarzadeh, S., Chen, Z., Li, S., Bobaru, F., 2019. A peridynamic mechano-chemical damage model for stress-assisted corrosion. Electrochim. Acta 323, 134795. http://dx.doi.org/10.1016/j.electacta.2019.134795.

Jafarzadeh, S., Zhao, J., Shakouri, M., Bobaru, F., 2022. A peridynamic model for crevice corrosion damage. Electrochim. Acta 401, 139512. http://dx.doi.org/10.1016/j.electacta.2021.139512.

Jame, Y.-W., Norum, D.I., 1980. Heat and mass transfer in a freezing unsaturated porous medium. Water Resour. Res. 16 (4), 811–819. http://dx.doi.org/10.1029/wr016i004p00811.

Karra, S., Painter, S., Lichtner, P., 2014. Three-phase numerical model for subsurface hydrology in permafrost-affected regions (PFLOTRAN-ICE v1. 0). Cryosphere 8 (5), 1935–1950.

Katiyar, A., Foster, J.T., Ouchi, H., Sharma, M.M., 2014. A peridynamic formulation of pressure driven convective fluid transport in porous media. J. Comput. Phys. 261, 209–229. http://dx.doi.org/10.1016/j.jcp.2013.12.039.

Kozlowski, T., 2004. Soil freezing point as obtained on melting. Cold Reg. Sci. & Technol. 38 (2–3), 93–101. http://dx.doi.org/10.1016/j.coldregions.2003.09.001.

Kumano, H., Asaoka, T., Saito, A., Okawa, S., 2007. Study on latent heat of fusion of ice in aqueous solutions. Int. J. Refrig. 30 (2), 267–273. http://dx.doi.org/10.1016/j.ijrefrig.2006.07.008.

Kurylyk, B.L., Hayashi, M., Quinton, W.L., Mckenzie, J.M., Voss, C.I., 2016. Influence of vertical and lateral heat transfer on permafrost thaw, peatland landscape transition, and groundwater flow. Water Resour. Res. 52 (2), 1286–1305. http://dx.doi.org/10.1002/2015wr018057.

Kurylyk, B.L., Watanabe, K., 2013. The mathematical representation of freezing and thawing processes in variably-saturated, non-deformable soils. Adv. Water Resour. 60, 160–177. http://dx.doi.org/10.1016/j.advwatres.2013.07.016.

Li, Z., Chen, J., Tang, A., Sugimoto, M., 2021. A novel model of heat-water-air-stress coupling in unsaturated frozen soil. Int. J. Heat Mass Transfer 175, 121375. http://dx.doi.org/10.1016/j.ijheatmasstransfer.2021.121375.

Li, W., Guo, L., 2021. Peridynamic investigation of chloride diffusion in concrete under typical environmental factors. Ocean Eng. 239, 109770. http://dx.doi.org/10.1016/j.oceaneng.2021.109770.

Li, Q., Sun, S., Xue, Y., 2010. Analyses and development of a hierarchy of frozen soil models for cold region study. J. Geophys. Res.: Atmos. 115 (D3), http://dx.doi.org/10.1029/2009JD012530.

Liu, P., Gu, X., Lu, Y., Xia, X., Madenci, E., Zhang, Q., 2023a. Peridynamics for mechanism analysis of soil desiccation cracking: Coupled hygro-mechanical model, staggered and monolithic solution. Comput. Methods Appl. Mech. Engrg. 406, 115896. http://dx.doi.org/10.1016/j.cma.2023.115896.

Liu, N., Li, N., Wang, S., Li, G., Song, Z., 2023b. A fully coupled thermo-hydro-mechanical model for fractured rock masses in cold regions. Cold Reg. Sci. & Technol. 205, 103707. http://dx.doi.org/10.1016/j.coldregions.2022.103707.

Liu, Z., Yu, X., 2011. Coupled thermo-hydro-mechanical model for porous materials under frost action: theory and implementation. Acta Geotech. 6 (2), 51–65. http://dx.doi.org/10.1007/s11440-011-0135-6.

Madenci, E., Barut, A., Dorduncu, M., 2019. Peridynamic Differential Operator for Numerical Analysis. Springer International Publishing, Cham, http://dx.doi.org/10.1007/978-3-030-02647-9.

Madenci, E., Oterkus, E., 2014. Peridynamic Theory and Its Applications, Vol. 9781461484. Springer New York, New York, NY, pp. 1–289. http://dx.doi.org/10.1007/978-1-4614-8465-3.

Mei, T., Zhao, J., Liu, Z., Peng, X., Chen, Z., Bobaru, F., 2021. The role of boundary conditions on convergence properties of peridynamic model for transient heat transfer. J. Sci. Comput. 87 (2), 50. http://dx.doi.org/10.1007/s10915-021-01469-0.

Michalowski, R.L., 1993. A constitutive model of saturated soils for frost heave simulations. Cold Reg. Sci. & Technol. 22 (1), 47–63. http://dx.doi.org/10.1016/0165-232X(93)90045-A.

Mizoguchi, M., 1990. Water, heat and salt transport in freezing soil (Ph.D. thesis). University of Tokyo (in Japanese).

Nassar, I.N., Horton, R., 1989. Water transport in unsaturated nonisothermal salty soil: II. Theoretical development. Soil Sci. Am. J. 53 (5), 1330–1337. http://dx.doi.org/10.2136/sssaj1989.03615995005300050005x.

Nassar, I.N., Horton, R., 1992. Simultaneous transfer of heat, water, and solute in porous media: I. Theoretical development. Soil Sci. Am. J. 56 (5), 1350–1356. http://dx.doi.org/10.2136/sssaj1992.03615995005600050004x.

Newman, G.P., Wilson, G.W., 1997. Heat and mass transfer in unsaturated soils during freezing. Can. Geotech. J. 34 (1), 63–70. http://dx.doi.org/10.1139/t96-085.

Nikolaev, P., Jivkov, A.P., Margetts, L., Sedighi, M., 2023. Non-local formulation of heat transfer with phase change in domains with spherical and axial symmetries. J. Peridynamics Nonlocal Model. http://dx.doi.org/10.1007/s42102-022-00092-3.

Nikolaev, P., Sedighi, M., Jivkov, A.P., Margetts, L., 2022. Analysis of heat transfer and water flow with phase change in saturated porous media by bond-based peridynamics. Int. J. Heat Mass Transfer 185, 122327. http://dx.doi.org/10.1016/j.ijheatmasstransfer.2021.122327.

Nimmo, J.R., Miller, E.E., 1986. The temperature dependence of isothermal moisture vs. Potential characteristics of soils. Soil Sci. Am. J. 50 (5), 1105–1113. http://dx.doi.org/10.2136/sssaj1986.03615995005000050004x.

Noborio, K., McInnes, K.J., Heilman, J.L., 1996. Two-dimensional model for water, heat, and solute transport in furrow-irrigated soil: II. Field evaluation. Soil Sci. Am. J. 60 (4), 1010–1021. http://dx.doi.org/10.2136/sssaj1996.03615995006000040008x.

Painter, S.L., 2011. Three-phase numerical model of water migration in partially frozen geological media: model formulation, validation, and applications. Comput. Geosci. 15 (1), 69–85. http://dx.doi.org/10.1007/s10596-010-9197-z.

Painter, S.L., Karra, S., 2014. Constitutive model for unfrozen water content in subfreezing unsaturated soils. Vadose Zone J. 13 (4), http://dx.doi.org/10.2136/vzj2013.04.0071, vzj2013.04.0071.

Peng, Z., Tian, F., Wu, J., Huang, J., Hu, H., Darnault, C.J.G., 2016. A numerical model for water and heat transport in freezing soils with nonequilibrium ice-water interfaces. Water Resour. Res. 52 (9), 7366–7381. http://dx.doi.org/10.1002/2016wr019116.

Philip, J.R., De Vries, D.A., 1957. Moisture movement in porous materials under temperature gradients. Trans. Am. Geophys. Union 38 (2), 222. http://dx.doi.org/10.1029/TR038i002p00222.

Saito, H., Šimůnek, J., Mohanty, B.P., 2006. Numerical analysis of coupled water, vapor, and heat transport in the vadose zone. Vadose Zone J. 5 (2), 784–800. http://dx.doi.org/10.2136/vzj2006.0007.

Santoyo, S.F., Baser, T., 2022. A review of the existing data on soil-freezing experiments and assessment of soil-freezing curves derived from soil–water retention curves. J. Cold Regions Eng. 36 (1), 04021020. http://dx.doi.org/10.1061/(ASCE)CR.1943-5495.0000271.

Sedighi, M., Yan, H., Jivkov, A.P., 2020. Peridynamics modelling of clay erosion. Géotechnique 1–12. http://dx.doi.org/10.1680/jgeot.20.P.149.

Sheshukov, A.Y., Nieber, J.L., 2011. One-dimensional freezing of nonheaving unsaturated soils: Model formulation and similarity solution: Freezing of nonheaving unsaturated soils. Water Resour. Res. 47 (11), http://dx.doi.org/10.1029/2011WR010512.

Silling, S., 2000. Reformulation of elasticity theory for discontinuities and long-range forces. J. Mech. Phys. Solids 48 (1), 175–209. http://dx.doi.org/10.1016/S0022-5096(99)00029-0.

Silling, S.A., Epton, M., Weckner, O., Xu, J., Askari, E., 2007. Peridynamic states and constitutive modeling. J. Elasticity 88 (2), 151–184.

Song, Y., Li, S., Zhang, S., 2021. Peridynamic modeling and simulation of thermo-mechanical de-icing process with modified ice failure criterion. Def. Technol. 17 (1), 15–35. http://dx.doi.org/10.1016/j.dt.2020.04.001.

Song, Y., Liu, R., Li, S., Kang, Z., Zhang, F., 2020. Peridynamic modeling and simulation of coupled thermomechanical removal of ice from frozen structures. Meccanica 55 (4), 961–976. http://dx.doi.org/10.1007/s11012-019-01106-z.

Stuurop, J.C., Van Der Zee, S.E., French, H.K., 2022. The influence of soil texture and environmental conditions on frozen soil infiltration: A numerical investigation. Cold Reg. Sci. & Technol. 194, 103456. http://dx.doi.org/10.1016/j.coldregions.2021.103456.

Stuurop, J.C., van der Zee, S.E.A.T.M., Voss, C.I., French, H.K., 2021. Simulating water and heat transport with freezing and cryosuction in unsaturated soil: Comparing an empirical, semi-empirical and physically-based approach. Adv. Water Resour. 149, 103846. http://dx.doi.org/10.1016/j.advwatres.2021.103846.

Taylor, G.S., Luthin, J.N., 1978. A model for coupled heat and moisture transfer during soil freezing. Can. Geotech. J. 15 (4), 548–555. http://dx.doi.org/10.1139/t78-058.

Tian, C., Fan, S., Du, J., Zhou, Z., Chen, Z., Bobaru, F., 2023. A peridynamic model for advection–reaction–diffusion problems. Comput. Methods Appl. Mech. Engrg. 415, 116206. http://dx.doi.org/10.1016/j.cma.2023.116206.

Tounsi, H., Rouabhi, A., Jahangir, E., 2020. Thermo-hydro-mechanical modeling of artificial ground freezing taking into account the salinity of the saturating fluid. Comput. Geotech. 119 (September 2019), 103382. http://dx.doi.org/10.1016/j.compgeo.2019.103382.

van Genuchten, M.T., 1980. A closed-form equation for predicting the hydraulic conductivity of unsaturated soils. Soil Sci. Am. J. 44 (5), 892–898. http://dx.doi.org/10.2136/sssaj1980.03615995004400050002x.

Vereecken, H., Schnepf, A., Hopmans, J., Javaux, M., Or, D., Roose, T., Vanderborght, J., Young, M., Amelung, W., Aitkenhead, M., Allison, S., Assouline, S., Baveye, P., Berli, M., Brüggemann, N., Finke, P., Flury, M., Gaiser, T., Govers, G., Ghezzehei, T., Hallett, P., Hendricks Franssen, H., Heppell, J., Horn, R., Huisman, J., Jacques, D., Jonard, F., Kollet, S., Lafolie, F., Lamorski, K., Leitner, D., McBratney, A., Minasny, B., Montzka, C., Nowak, W., Pachepsky, Y., Padarian, J., Romano, N., Roth, K., Rothfuss, Y., Rowe, E., Schwen, A., Šimůnek, J., Tiktak, A., Van Dam, J., van der Zee, S., Vogel, H., Vrugt, J., Wöhling, T., Young, I., 2016. Modeling soil processes: Review, key challenges, and new perspectives. Vadose Zone J. 15 (5), 1–57. http://dx.doi.org/10.2136/vzj2015.09.0131.

Wang, B., Oterkus, S., Oterkus, E., 2022. Thermomechanical phase change peridynamic model for welding analysis. Eng. Anal. Bound. Elem. 140, 371–385. http://dx.doi.org/10.1016/j.enganabound.2022.04.030.

Wang, Y., Zhou, X., Kou, M., 2018. Peridynamic investigation on thermal fracturing behavior of ceramic nuclear fuel pellets under power cycles. Ceram. Int. 44 (10), 11512–11542. http://dx.doi.org/10.1016/j.ceramint.2018.03.214.

Wang, Y., Zhou, X., Kou, M., 2019. An improved coupled thermo-mechanic bond-based peridynamic model for cracking behaviors in brittle solids subjected to thermal shocks. Eur. J. Mech. A Solids 73, 282–305. http://dx.doi.org/10.1016/j.euromechsol.2018.09.007.

Watanabe, K., Kito, T., Dun, S., Wu, J.Q., Greer, R.C., Flury, M., 2013. Water infiltration into a frozen soil with simultaneous melting of the frozen layer. Vadose Zone J. 12 (1), http://dx.doi.org/10.2136/vzj2011.0188, vzj2011.0188.

Watanabe, K., Wake, T., 2009. Measurement of unfrozen water content and relative permittivity of frozen unsaturated soil using NMR and TDR. Cold Reg. Sci. & Technol. 59 (1), 34–41. http://dx.doi.org/10.1016/j.coldregions.2009.05.011.

Wu, P., Liu, Y., Peng, X., Chen, Z., 2022. Peridynamic modeling of freeze-thaw damage in concrete structures. Mech. Adv. Mater. Struct. 1–12. http://dx.doi.org/10.1080/15376494.2022.2064015.

Yan, H., Jivkov, A.P., Sedighi, M., 2021a. Modelling the soil desiccation cracking by peridynamics. Géotechnique 1–35. http://dx.doi.org/10.1680/jgeot.21.00032.

Yan, H., Sedighi, M., Jivkov, A.P., 2020. Peridynamics modelling of coupled water flow and chemical transport in unsaturated porous media. J. Hydrol. 591 (October), 125648. http://dx.doi.org/10.1016/j.jhydrol.2020.125648.

Yan, H., Sedighi, M., Jivkov, A., 2021b. Modelling the effects of water chemistry and flowrate on clay erosion. Eng. Geol. 294, 106409. http://dx.doi.org/10.1016/j.enggeo.2021.106409.

Zhang, S., Teng, J., He, Z., Liu, Y., Liang, S., Yao, Y., Sheng, D., 2016a. Canopy effect caused by vapour transfer in covered freezing soils. Géotechnique 66 (11), 927–940.

Zhang, S., Teng, J., He, Z., Sheng, D., 2016b. Importance of vapor flow in unsaturated freezing soil: a numerical study. Cold Reg. Sci. & Technol. 126, 1–9. http://dx.doi.org/10.1016/j.coldregions.2016.02.011.

Zhang, X., Wang, Q., Yu, T., Wang, G., Wang, W., 2018. Numerical study on the multifield mathematical coupled model of hydraulic-thermal-salt-mechanical in saturated freezing saline soil. Int. J. Geomech. 18 (7), 04018064. http://dx.doi.org/10.1061/(ASCE)GM.1943-5622.0001173.

Zhang, M., Wen, Z., Xue, K., Chen, L., Li, D., 2016c. A coupled model for liquid water, water vapor and heat transport of saturated–unsaturated soil in cold regions: model formulation and verification. Environ. Earth Sci. 75 (8), http://dx.doi.org/10.1007/s12665-016-5499-3.

Zhao, J., Chen, Z., Mehrmashhadi, J., Bobaru, F., 2018. Construction of a peridynamic model for transient advection-diffusion problems. Int. J. Heat Mass Transfer 126, 1253–1266. http://dx.doi.org/10.1016/j.ijheatmasstransfer.2018.06.075.

Zheng, C., Chen, Y., Gao, W., Liang, X., Simunek, J., Liu, X., 2023. Water transfer mechanisms and vapor flow effects in seasonally frozen soils. J. Hydrol. 627, 130401. http://dx.doi.org/10.1016/j.jhydrol.2023.130401.

Zheng, T., Miao, X.-Y., Naumov, D., Shao, H., Kolditz, O., Nagel, T., 2022. A thermo-hydro-mechanical finite-element model with freezing processes in saturated soils. Environ. Geotech. 9 (8), 502–514. http://dx.doi.org/10.1680/jenge.18.00092.

Zheng, C., Simunek, Y., Lu, Y., Liu, X., Shi, C., Li, H., Yu, L., Zeng, Y., Su, Z., 2021. Development of the Hydrus-1D freezing module and its application in simulating the coupled movement of water, vapor, and heat. J. Hydrol. 598, 126250. http://dx.doi.org/10.1016/j.jhydrol.2021.126250.

Zhou, X.-P., Wang, Y.-T., 2021. State-of-the-art review on the progressive failure characteristics of geomaterials in peridynamic theory. J. Eng. Mech. 147 (1), 03120001. http://dx.doi.org/10.1061/(ASCE)EM.1943-7889.0001876.

Zhou, Y., Zhang, M., Pei, W., Wang, Y., 2022. A non-local frost heave model based on peridynamics theory. Comput. Geotech. 145, 104675. http://dx.doi.org/10.1016/j.compgeo.2022.104675.

Zhou, Y., Zhou, G., 2010. Numerical simulation of coupled heat-fluid transport in freezing soils using finite volume method. Heat Mass Transf. 46 (8–9), 989–998. http://dx.doi.org/10.1007/s00231-010-0642-2.

Zhou, X., Zhou, J., Kinzelbach, W., Stauffer, F., 2014. Simultaneous measurement of unfrozen water content and ice content in frozen soil using gamma ray attenuation and TDR. Water Resour. Res. 50 (12), 9630–9655. http://dx.doi.org/10.1002/2014WR015640.